

POLITECNICO
MILANO 1863

Falcon9 - Spacecraft structural compliance analysis

Space Strutto Group:

Dan Borcea (10678208)

Pietro Bosco (10643020)

Orlando Pietromarchi (10601697)

Daniele Peruzzotti (10702005)

Matteo Cuccaro (10604872)

Final Report

Course of Analysis and Testing of Space Structures
School of Industrial Engineering
Academic Year 2023-2024

Acronyms

Acronym	Meaning
APSD	Acceleration Power Spectral Density
CLA	Coupled Load Analysis
COG	Centre Of Gravity
CTE	Coefficient of Thermal Expansion
DOF	Degree Of Freedom
ERS	Extreme Response Spectrum
ESI	Equivalent SIne Input
IF	Interface
IUT	Item Under Test
LM	Large Mass
LV	Launcher Vehicle
MLI	Multi Layer Insulation
MoS	Margin of Safety
OASPL	OverAll Sound Pressure Level
PL	Payload
PPSD	Pressure Power Spectral Density
QS	Quasi Static
QSL	Quasi Static Load
SC	Spacecraft
SF	Safety Factor
SRS	Shock Response Spectrum
UM	User Manual

Contents

1 LV and SC modelling	1
1.1 Launch vehicle	1
1.1.1 General aspects	1
1.1.2 Fairing available volume	2
1.1.3 Center of gravity constraint	2
1.2 Spacecraft	3
1.2.1 General aspects	3
1.2.2 Main components	4
1.3 SC compliance with respect to basic requirements	6
2 Modal analysis	7
2.1 Process design	7
2.2 Natural frequencies requirement	7
2.3 Launcher tuning process and results	8
2.4 Spacecraft tuning process and results	9
2.5 Launcher and spacecraft modal analysis	11
3 Static analysis	12
3.1 Process design	12
3.2 Line loads and overfluxes	12
3.3 Results	13
3.4 Clamp band tension assessment	15
4 Dynamic coupling	16
4.1 Process design	16
4.2 Dynamic coupling model: Large Mass method	16
4.3 Results	18
5 Thermoelastic analysis	20
5.1 Introduction	20
5.2 Thermoelastic model	20
5.3 Results	23
6 Sine testing	26
6.1 Process design	26
6.2 Primary notching	27
6.3 Secondary notching	27
6.4 ESI	27
6.5 Results	28

7 Acoustic testing	30
7.1 Introduction	30
7.2 Qualification standards	32
7.3 Process design	33
7.4 Results	34
8 Severity Comparison	36
9 Buckling analysis	39
9.1 Introduction	39
9.2 Buckling model	39
9.3 Results	40
10 Summary of requirements	44

List of Figures

1.1	Falcon 9 launcher	1
1.2	Falcon 9 mesh model	2
1.3	Falcon 9 mesh and dimensions	2
1.4	Allowable COG height above the 2624mm plane	3
1.5	Section view of the spacecraft	4
1.6	Solar panels details	5
1.7	Solar panels details	5
1.8	Spacecraft inside the fairing	6
2.1	Launcher principal modes	9
2.2	Spacecraft principal modes	11
3.1	Falcon 9 flight limit load factors for “standard” mass payloads (over 1841 kg)	12
3.2	Fluxes for $QSL_{long} = 0$ and $QSL_{lat} = 2.5$; Overflux = -3.1 %	14
3.3	Fluxes for $QSL_{long} = -7.5$ and $QSL_{lat} = 0$; Overflux = +1.7 %	14
4.1	Simplified model of the Falcon 9’s coupled system	16
4.2	LV-SC dynamic coupling transmissibility	18
4.3	LV-SC dynamic coupling transmissibility	19
4.4	T_{max} evolution for different SC frequencies	19
5.1	Thermoelastic model	21
5.2	Thermal map of SC	23
5.3	Thermal map of SC’s inner components	23
5.4	Deformation due to thermoelastic effects	24
5.5	Deformation of the inner components due to thermoelastic effects	25
6.1	Sinusoidal vibration levels for a single launch configuration [1]	26
6.2	Input forces for the CLA	28
6.3	Sine X test prediction results	29
6.4	Sine Y test prediction results	29
6.5	Sine Z test prediction results	29
7.1	GSFC standard, [5]	32
7.2	Acceleration power spectral density	35
8.1	Severity comparison	38
9.1	Buckling mode: $\lambda_{min} = 29.95881$	41
9.2	Buckling mode: $\lambda_{min} = 28.01055$	41

9.3	Buckling mode: $\lambda_{min} = 40.04872$	41
9.4	Buckling mode: $\lambda_{min} = 28.51616$	42
9.5	Buckling mode: $\lambda_{min} = 28.74921$	42
9.6	Buckling mode: $\lambda_{min} = 39.42682$	42
9.7	Buckling mode: $\lambda_{min} = 27.55283$	43

List of Tables

1.1	F9 mass distribution	1
1.2	Material properties	1
1.3	List of materials and thickness for the spacecraft	4
2.1	List of properties and materials for the launcher subsystem	8
2.2	Results of the LV tuning process	8
2.3	List of properties and materials for the spacecraft subsystem	10
2.4	Results of the SC tuning process	10
2.5	Modal analysis of spacecraft and launch vehicle	11
2.6	Modal analysis results for the SC coupled to LV	11
3.1	Overflux computation	14
3.2	Maximum tensional line loads	15
5.1	Thermal nodes coordinates and temperatures for temperature gradient along X axis	21
5.2	Thermal nodes coordinates and temperatures for temperature gradient along Y axis	22
5.3	SC's coefficients of thermal expansion	22
5.4	Absolute rotations	24
5.5	Relative rotations	24
6.1	Limits on the lateral moments and axial force	27
6.2	Antenna qualification levels	27
7.1	Acoustic vibration qualification level	30
7.2	Nastran input computation	31
8.1	Qualification loads for the unit	36
8.2	Severity comparison summary	38
9.1	QLS and λ_{min} values	40
10.1	Recapitulation of all the analysis	44

Chapter 1

LV and SC modelling

1.1 Launch vehicle

1.1.1 General aspects

Falcon 9 is a family of partially reusable launch vehicles capable of carrying heavy payloads to low elliptical orbit and geosynchronous orbit as well, for the latest version up to 22800 kg in the first case and up to 8300 kg in the latter. It is divided into two stages separated by an interstage component, housing the pneumatic pushers that allow the first and second stage to separate during flight. Onto it four grid fins are attached, whose mass was estimated to be 200 kg . For the modelling of the Falcon 9, in this analysis the launch vehicle was subdivided into: first stage, interstage, second stage, adapter and fairing. In Tab. 1.1, each subsystem of the launcher is represented by its relative wet mass, except for the interstage, whose mass is unknown.

Table 1.1: F9 mass distribution

Subsystem	Mass [kg]
First stage	420000
Second stage	96000
Adapter	1865
Fairing	3700
Grid fin	200

Figure 1.1: Falcon 9 launcher



Assuming that this analysis of the structure is being undertaken in a very preliminary phase of the design, the different parts of the launch vehicle are not modeled into detail. In order to be compliant with the general weight of the launcher, the only parameters which are being tuned to represent the mass of the system are the material density and the wall thickness. Hence, the entire launcher shape is approximated using a plate model.

Subsystem	Material density [kg/m ³]	Wall thick- ness [cm]
First stage	8803	10
Second stage	5845	10
Interstage	23933	1.5
Adapter	5000	3
Fairing	383	2.5

Table 1.2: Material properties

Each component of the launcher mentioned before is represented by its own material and wall thickness. In Tab. 1.2, the chosen values are shown.

The total wet mass declared by the launcher user manual is around 550000 kg , while the sum of the masses from the table above is significantly smaller; thus, the remaining 30 tons were allocated to the interstage subsystem. By doing so, both the general system and each individual section of the launcher are quite representative of the mass distribution of the Falcon 9. The four grid fins were modeled as 200 kg concentrated masses.

The model of the launcher was defined in a way such that it is quite representative of the real structure. In particular, the height of the whole system, the main diameter of the first and second stage, the maximum diameter of the fairing and some axial dimensions of the two stages were taken as a reference, while all the other dimensions, such as the shape of the nozzles and the curvature of the fairing, were chosen in a qualitative way. The diameter of the adapter was set equal to the Falcon 9's 2624mm payload attach fitting, which allows launching into space payloads weighting more than 1815 kg .

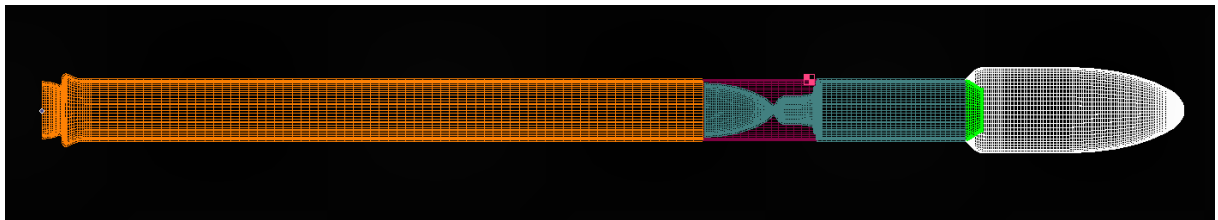


Figure 1.2: Falcon 9 mesh model

1.1.2 Fairing available volume

The standard SpaceX Falcon fairing is 5.2 m wide in outer diameter and 13.2 m high overall, as shown in Fig. 1.3. One of the first checks to be done in order to verify the compliance of the spacecraft with the launcher interface is to make sure that the whole body of the space structure is completely enclosed by the walls of the fairing, possibly with a certain margin.

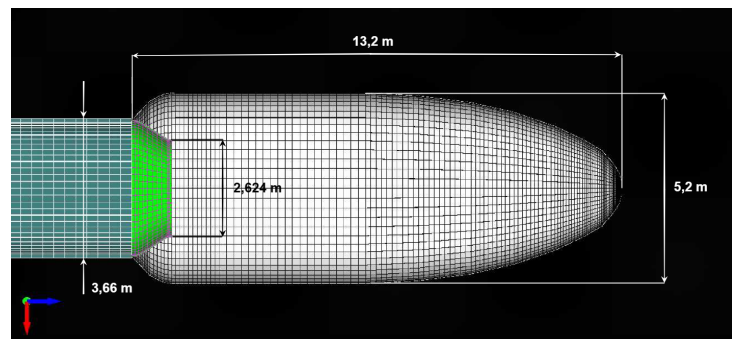


Figure 1.3: Falcon 9 mesh and dimensions

1.1.3 Center of gravity constraint

The launcher user manual clearly specifies a limit for the distance between the center of gravity of the spacecraft and the adapter interface as a function of the mass of the spacecraft. In Fig. 1.4, the relation is shown for the chosen adapter.

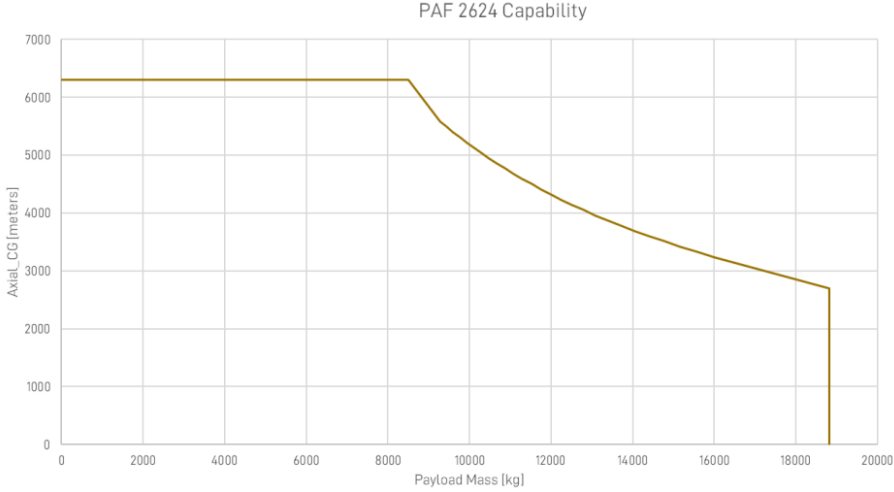


Figure 1.4: Allowable COG height above the 2624mm plane

In this chart the COG distance is expressed in millimeters. It is pretty clear that the function is characterized by a hyperbolic shape. This is because the bending moment at the interface and the resultant lateral force applied to the spacecraft in the center of gravity are directly proportional to each other, and since the force can be written as the product of mass and acceleration of the spacecraft, the following expression is true:

$$M = m a_{sc} x_{COG} \quad (1.1)$$

Since the mass of the spacecraft is significantly lower than the launcher's mass and since the spacecraft is stiffly connected to the launch vehicle by the adapter, its acceleration is almost equal to the acceleration of the system and is strictly dependent on the flight envelope, which can be estimated a priori and increased by a factor to be more conservative. At this point, in order to limit the bending moment at the interface between spacecraft and launcher below a certain value, a limit to the product between the mass and x_{COG} shall be imposed. This is the reason why they are inversely proportional. The model of the spacecraft will have to respect this relation.

1.2 Spacecraft

1.2.1 General aspects

Unlike the launch vehicle, a certain amount of attention to the details was given to the spacecraft, since it has been the main target of most of the analyses. Another reason for this choice was the desire of dividing the model into some structural components, with the goal of keeping everything together, and some functional components, such as payload, the tanks, and the external cover, which are not subjected to relatively elevated stresses during the flight. In this way, during the modal analysis it was possible to tune each component individually in a more realistic way, without enforcing excessively the entire system, which would have led to adding inert mass to the payload. The modelling of the spacecraft was performed in an iterative way, each time the mesh of the spacecraft was completed, based on the results of the following analysis, it got updated in such a way to satisfy the requirements for the outputs of the analysis.

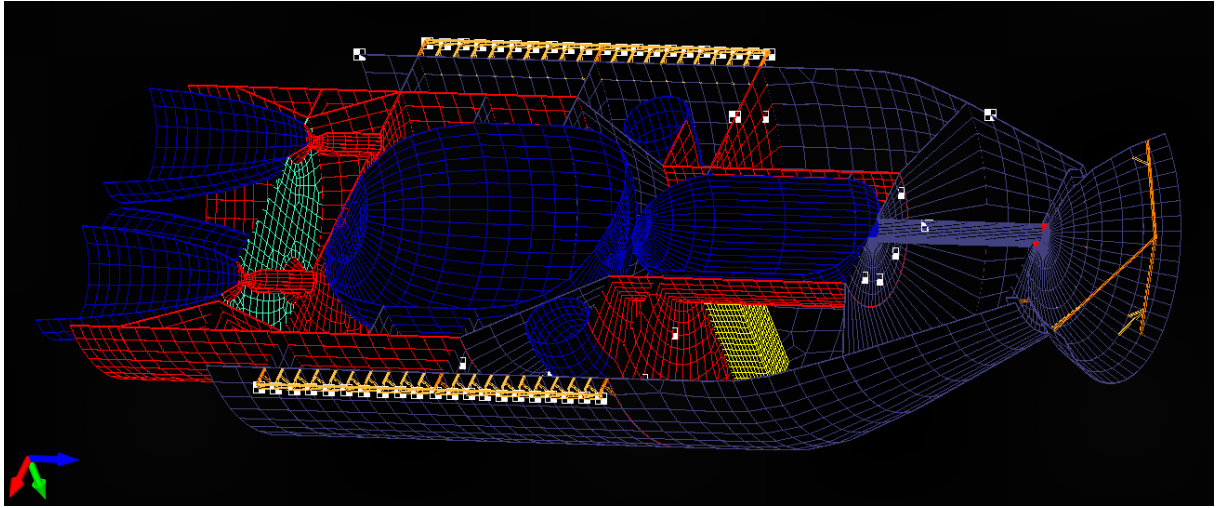


Figure 1.5: Section view of the spacecraft

For example, great attention was given to the constraints of the modal analysis and to the static analysis, as it will be explained in next chapters. During the process different solutions were adopted in order to change the results of the analysis. Figure 1.5 shows the cross section view of the final configuration of the space structure: a spacecraft design including its own propulsive system, composed by four engines and three tanks (propellant, oxidizer and pressurizing gas tank, one of them is characterized by a toroidal shape), an antenna, a telescope, 2 solar panels whose masses are represented by an amount of concentrated masses equally distributed, and some additional concentrated masses as a replacement for other payload components, actuators and sensors, for example the star trackers. In Tab. 1.3, the material density and wall thickness for each component are listed.

Table 1.3: List of materials and thickness for the spacecraft

Subsystem	Color	Material density [kg/m ³]	Wall thickness (or beam radius) [cm]
Main structure	red	5000	1
Engine enforcing plate	green	7000	1
Engine and tanks	blue	4000	0.5
Cover	violet	1500	0.6
Telescope	yellow	2700	2
Stiffer beams	dark orange	7000	1
Weaker beams	light orange	3000	0.8

1.2.2 Main components

Structure

The main structural components of the spacecraft are indicated by the red colour. This group of elements is characterized by one of the highest values for density, young modulus and bending stiffness factor and it's main goal is to give a certain stiffness to the spacecraft. The fact that it is assembled over the adapter through a cylindrical component gives the

possibility of avoiding extremely high overfluxes in the static analysis, since the entire load is released on the adapter interface longitudinally without bending moments. This is a pretty frequent configuration in real space structures. The reason behind the existence of the additional green structural plate will be discussed in the next chapter.

Tanks and engines

They are supposed to be subjected to minor stresses with respect to the structure. A still relevant density was assigned to them in order to take count of the propellant mass and of the architecture of the propulsive system. The engines were split between their representative material and the structural material.

Covering material

It is characterized by the lowest values of density and stiffness since almost no structural enforcement is given by them.

Payload

Some payload components were modeled for the analysis. The two solar panels were modeled using 60 concentrated masses equally distributed over a complex of beams. The latter ones are constrained either to the external covering wall or to one of the three available horizontal plates, as it can be seen in the Fig. 1.6. Many attachment points are used to fix the solar panels in order to avoid concentrated stresses on the covering surface. For the same reason the beams constrained to the cylindrical covering surface have a minor young modulus and density with respect to the ones which are stressing longitudinally the horizontal surfaces. In order to fully constrain the radially disposed beams some additional lateral ones are needed at both ends to avoid rotation. The telescope was modeled as a box where one of the faces is attached to one of the horizontal surfaces, while a cylindrical part was extruded until it protruded from the covering surface, as displayed in Fig. 1.7. The parabolic shape of the antenna was meshed using the same material as the fuselage but four structural beams, with additional lateral beams to avoid free rotation, were added in order to simulate the receiver in front of the parabola and its structural holding beams.

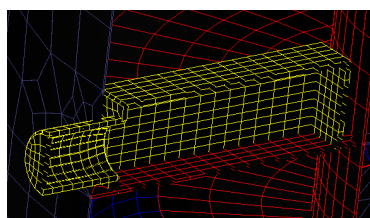


Figure 1.7: Solar panels details

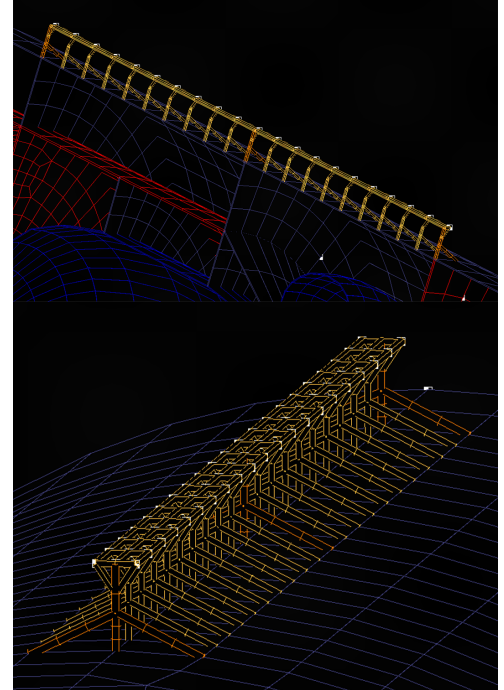


Figure 1.6: Solar panels details

Other payload components and actuators were modeled as concentrated masses, uniformly distributed on the horizontal surfaces, as it can be seen in Fig. 1.5.

1.3 SC compliance with respect to basic requirements

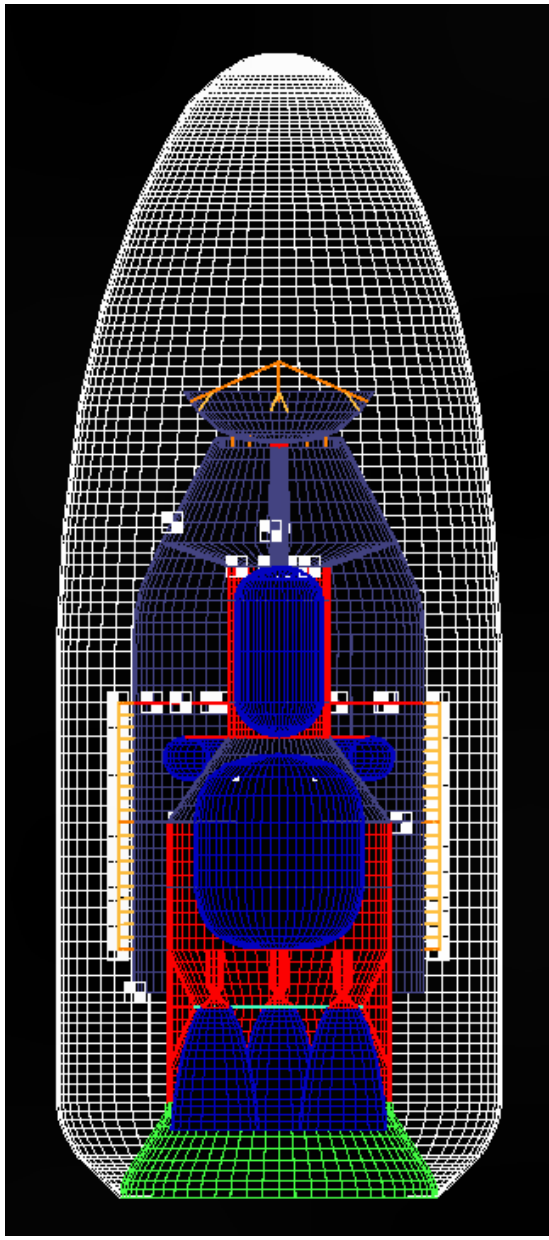


Figure 1.8: Spacecraft inside the fairing

A summary of all the above cited requirements can be made in order to check their fulfillment by the spacecraft. In Fig. 1.8, it is quite obvious that the model of the spacecraft is easily included inside the volume of the fairing. Also in this figure it can be seen the coupling of the spacecraft with the Falcon 9 default adapter. The value of the mass of the entire spacecraft is 8525.5 kg , which is well above the lower limit (1815 kg) of the 2624mm-PAF and well below the maximum payload capacity given by the Falcon 9 (22000 kg). Regarding the center of gravity its axial distance from the interface of the adapter is 3.546 m , which is below the maximum allowable distance value for the respective mass, around 6.2 m , as shown in Fig. 1.4. The space structure is also almost fully axial symmetrical, leading to a center of gravity which is positioned very close to the longitudinal axis of the launch vehicle, with a 1.05 cm displacement, avoiding in this way the additional bending moment contribution from the axial forces.

Chapter 2

Modal analysis

2.1 Process design

A modal analysis was performed in order to ensure that the natural frequencies of both the LV and the SC met the requirements imposed by the launcher authority; during the qualification of a space structure to be launched into space, one of the fundamental conditions that needs to be satisfied is the frequency decoupling of the launcher vehicle and the spacecraft, as well as to avoid harmonic resonances which would cause severe damages to the structure.

Once the requirements are set, the LV and SC parameters shall be tuned. Firstly, the frequencies of the launcher were computed through a F-F (Free-Free) modal analysis on the model of the launcher, exploiting the `template 103 modal run` code. Afterward, a H-M (Hard-Mounted) modal analysis was performed on the spacecraft's model, where the nodes at the interface between LV and SC were fixed along all six DOFs; this was done through the `103 HM SC` code. Both the F-F and the H-M analyses were conducted in MSC Nastran. Lastly, an F-F analysis of the LV and SC connected at the interface nodes was performed in order to check the consistency of the results obtained previously. The LV frequency values are not expected to vary significantly, as the SC mass is small with respect to the LV's one; regarding SC, if the frequencies are similar to the ones computed through the H-M analysis, then the consistency of the results is proved.

2.2 Natural frequencies requirement

The Falcon 9 users guide states that the primary natural frequency along the lateral axis of the spacecraft, after being constrained to the adapter interface, must be above 10 Hz, while regarding the longitudinal motion the minimum allowed primary frequency is 25 Hz. Furthermore, the launcher user's manual states another constraint which has to be imposed on the frequency content: all the secondary modes of the spacecraft must be characterized by a resonant frequency which has to be greater than 35 Hz. In other words, the primary modes of the whole structure must overcome before individual components of the spacecraft resonate. To all these requirements an additional margin should be applied in order to be more conservative and to avoid any partial resonance which can overcome when the external loads are exciting the system with a frequency which is in the middle and very close to the natural frequencies of the launcher and spacecraft.

Since the frequency content requirements for the spacecraft are given, the range for the resonant frequencies of the launch vehicle shall be complementary to the range of fre-

quencies of the spacecraft. Thus the longitudinal mode of the launcher vehicle should be represented by a resonant frequency well below 25 Hz while the resonance of lateral mode should manifest well below 10 Hz.

2.3 Launcher tuning process and results

As mentioned before the launch vehicle was divided into: first stage, interstage, second stage, adapter and fairing. To each component some material and plate properties were given. Since the entire structure was modeled using plates, the two parameters that were tuned to represent the plate property were the wall thickness and the bending stiffness ratio. To represent the material, other than the previously cited density, the parameters that were tuned in order to respect the requirements are the young modulus and the shear modulus. The Poisson number was fixed to 0.299 for all the materials. Representing a specific material was not a driving factor in choosing these parameters but much more important was to respect the total mass of the respective components and the admissible frequency range from the previous section. In Tab. 2.1 below it is possible to visualize all the plate properties and the related material for each subsystem.

Table 2.1: List of properties and materials for the launcher subsystem

Subsystem	Young modulus [GPa]	Shear modulus [GPa]	Bending stiffness factor [-]	Density [kg/m ³]	Wall thickness [cm]
First stage	24	28	1700	8803	10
Interstage	75	28	2000	23933	1,5
Second stage	24	20	1700	5845	10
Adapter	24	20	2600	5000	3
Fairing	10	20	1700	383	2,5

The bending stiffness ratio represents an additional enforcement of the plate in order to better resist to bending moments from loads.

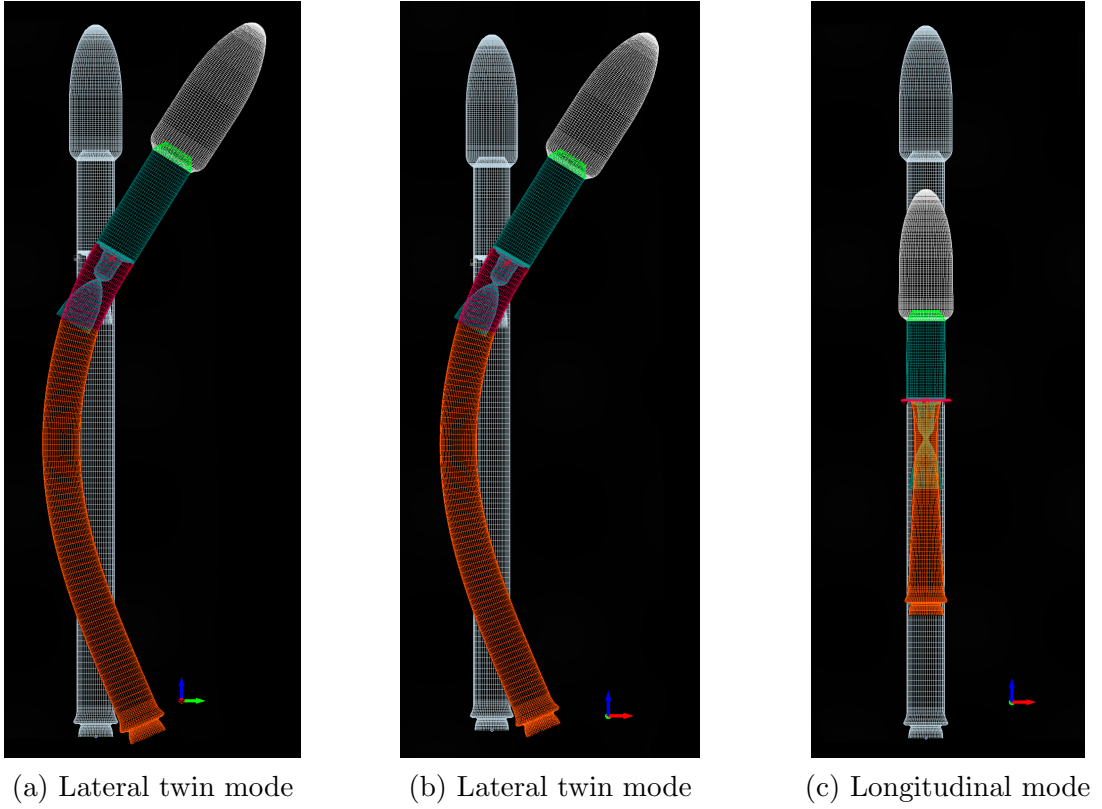
Once the model parameters were set, the modal analysis was performed and the values of the natural frequencies were computed as shown in Tab. 2.2; it is clear that both the primary longitudinal and the lateral natural frequencies meet the requirements imposed earlier.

Table 2.2: Results of the LV tuning process

Mass [kg]	Lateral freq. [Hz]	Longitudinal freq. [Hz]
549772	2.640552	14.13171

Finally, a visual representation of the lateral and longitudinal vibration modes of the launcher vehicle is displayed in Fig. 9.7a, 9.7b and 9.7c:

Figure 2.1: Launcher principal modes



2.4 Spacecraft tuning process and results

While the modelling and the tuning process of the launcher vehicle didn't imply serious problems, the same process related to the spacecraft was much more challenging. One of the major problems for example was to satisfy the third natural frequency requirement: all secondary modes shall overcome at frequencies higher than 35 Hz and after the principal modes of the entire spacecraft. While the original goal of having a specialized material and plate property for the main structure of the spacecraft was to make it stiffer in order to make sure that the first natural frequencies were higher than the requirement, in the end the result was that these frequencies were much higher than the minimum threshold, above 120 Hz, while some secondary modes were overcoming at lower frequencies. Along these secondary modes one of the most imminent was the lateral motion of the engines and the bending of the horizontal plates holding them. The engines were originally made of the same material of the main structure. Although decreasing the bending stiffness ratio of the structure would help on decreasing the principal natural frequencies of the whole system, also the secondary modes of the engines would be affected, thus some other solutions were adopted:

- to the divergent part of the nozzle a lighter material was allocated, in order to reduce the inertia of the engine, since the resonance frequency of the mode generally is inversely proportional to the implied inertial mass;
- considering the horizontal plate holding the engines, the central part, which is in direct contact with the four combustion chambers, was reinforced with a new ma-

terial, with even higher bending stiffness ratio and density, as already stated in the previous chapter;

- the entire horizontal surface was additionally reinforced by adding an axisymmetric bracing like structural component, in order to reduce the internal bending stress.

By applying these solutions to the mesh model it was possible to keep constant the frequency range of the secondary mode while reducing the principal longitudinal mode of the spacecraft below it, which was obtained by reducing the young modulus and the bending stiffness ratio of the main structural material.

Similar problems were triggered by the modelling of the antenna and of the solar panels. Also in these cases the secondary modal frequencies related to the oscillations of the interested components were lower than the principal resonance frequencies of the spacecraft. In the first case the problem was solved by adding several stiffening beam components along the perimeter of the antenna. In the latter one the problem was caused by the attachments of the heavy and inertial solar panel structure to the very soft external panels of the spacecraft. To solve this the number of the beam components constraining the panels to the spacecraft was increased while their density and young modulus were decreased, in order to better distribute the internal stresses.

Table 2.3: List of properties and materials for the spacecraft subsystem

Subsystem	Young modulus [GPa]	Shear modulus [GPa]	Bending stiffness factor [-]	Density [kg/m ³]	Wall thickness [cm]
Main structure	60	20	700	5000	1
Enforcing base	180	38	5000	7000	1
External panels	15	18	50	1500	0.6
Tanks and nozzles	30	20	200	4000	0.5
Telescope	65	27	2	2700	2
Weak beams	45	21	-	3000	0.8
Stiff beams	120	40	-	7000	1

The results of the modal analysis on the model of the spacecraft are shown in Tab. 2.4. It is important to point out that the two primary lateral frequencies marginally differ as the SC model is not perfectly symmetric, in contrast to the model of LV.

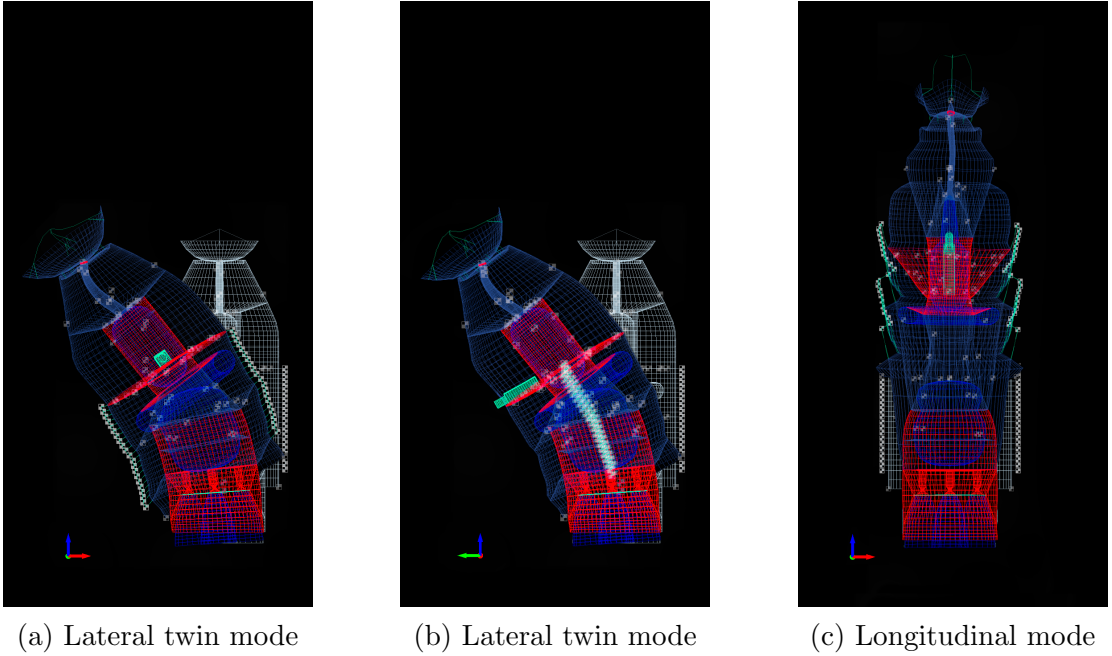
Table 2.4: Results of the SC tuning process

Mass [kg]	1 st lateral freq.	2 nd lateral freq.	Longitudinal freq.	Secondary freq.
8525.5	14.31699 Hz	14.37821 Hz	32.50622 Hz	39.08669 Hz

The vibration modes related to the computed frequencies are portrayed in Fig. 2.2a, 2.2b and 2.2c. All the requirements are satisfied:

- The principal lateral frequencies are above 10 Hz with a reasonable margin;
- The frequency of the principal longitudinal mode is above 25 Hz and below the modal frequency of the first secondary mode with margin;
- All secondary modes are characterized by resonance frequencies higher than 35 Hz.

Figure 2.2: Spacecraft principal modes



2.5 Launcher and spacecraft modal analysis

Finally, the same modal simulation could be done for the whole system. The natural frequencies of the principal modes are shown in the Table below:

Table 2.5: Modal analysis of spacecraft and launch vehicle

	Mass [kg]	1 st lateral freq.	2 nd lateral freq.	Longitudinal freq.
Single	549772.1	2.640552 Hz	2.640552 Hz	14.13171 Hz
Coupled	558298.6	2.418004 Hz	2.418308 Hz	13.78203 Hz

As expected, since the mass of the spacecraft is much smaller than the mass of the launch vehicle, the modal frequencies of the launcher coupled to the spacecraft are not so different from the ones from the analysis of the launcher by itself. All principal resonance frequencies are slightly lower because by adding an additional mass to the system, the general inertia of it is higher, thus affecting negatively the general modal frequencies. In the table below it can be seen how the modal frequencies of the SC are being affected by the coupling with the LV.

Table 2.6: Modal analysis results for the SC coupled to LV

	1 st lateral freq.	2 nd lateral freq.	Longitudinal freq.	Secondary freq.
Single	14.31699 Hz	14.37821 Hz	32.50622 Hz	39.08669 Hz
Coupled	13.01755 Hz	13.04743 Hz	32.01025 Hz	36.96306 Hz

Chapter 3

Static analysis

3.1 Process design

The aim of the static test should be to confirm that the structure survives with no damage nor degradation to qualification QS loads declared in the LV user manual and, more in general, to the unit/equipment IF forces predicted for the entire mechanical qualification test campaign. This is done by applying several load cases, often in different directions, using a shaker to make the structure reach specified accelerations. To guarantee the QS nature of the loading, the excitation imposed must have a frequency content significantly lower than the first resonance frequency of the structure. The QSLs are accelerations typically expressed in g , generating IF forces and moments equivalent to the ones coming from more complex loadings, not necessarily static but, where also the dynamics may play a crucial role. They are useful as they allow to verify the structure without running complex dynamic analysis.

3.2 Line loads and overfluxes

The flight envelope of Falcon 9 is shown in Fig. 3.1 [1]; it represents the limit combinations between axial and lateral accelerations that the structure can withstand. Here a positive axial acceleration represents compression, while a negative value represents tension. The combinations of loads chosen for the following analysis are the ones representing the points that build the perimeter of the envelope. The lateral loads are intended to be applied once along the spacecraft x -axis and once along the spacecraft y -axis, therefore each point has to be considered twice. The diameter of the adapter, the

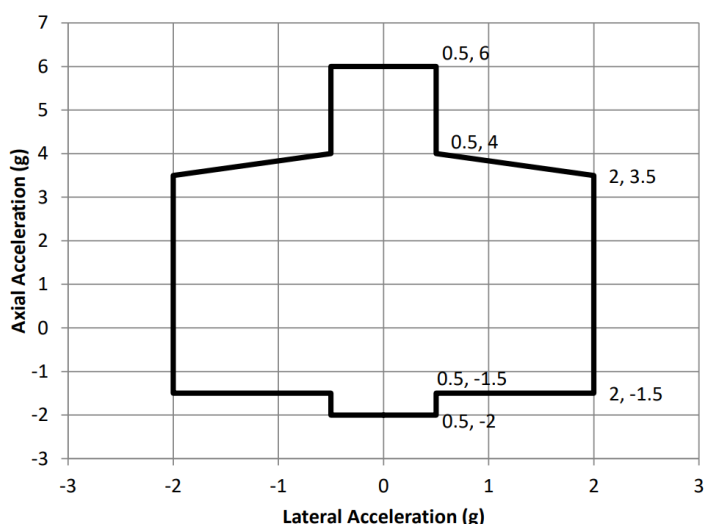


Figure 3.1: Falcon 9 flight limit load factors for “standard” mass payloads (over 1841 kg)

height of the spacecraft's center of mass with respect to the interface and the spacecraft's mass are $D_{if} = 2.624\text{ m}$, $z_{CoG} = 3.546\text{ m}$ and $m_{sc} = 8525.5\text{ kg}$. Overfluxes should never exceed the 10 % value. For each point of the envelope the longitudinal interface force F_N and the lateral interface moment M_{lat} can be calculated [2] as:

$$F_N = m_{sc}QSL_{long}SF \quad M_{lat} = m_{sc}QSL_{lat}z_{CoG}SF \quad (3.1)$$

Where SF is the safety factor, assumed as 1.25 in agreement with the LV user manual. If F_N , M_x and M_y are all simultaneously present, the following equation can be written to obtain the overall resulting line load:

$$f_{overall} = \frac{F_N}{\pi D_{if}} + 4 \frac{M_x}{\pi D_{if}^2} \cos\left(\theta - \frac{\pi}{4}\right) + 4 \frac{M_y}{\pi D_{if}^2} \cos\theta \quad (3.2)$$

Where θ is the angular coordinate of the interface ring, starting from x and counter-clockwise. The so calculated $f_{overall}$ is the line load analytically calculated under the hypothesis of circular ring, axial-symmetrical structure and that the lateral moments are generated only from the longitudinal line load along the z-axis. This results are useful to make the comparison with the corresponding line loads numerically calculated from the FE model of the spacecraft, which gives the more accurate values. FE calculations, indeed, take into account discontinuities and differences in the local stiffness, as well as asymmetries of the structure. Overfluxes would in fact become very large in the case of a very non-symmetric spacecraft. From the FE model, real fluxes are calculated running a static analysis on *MSC Nastran* applying a *1g* load along one axis at a time. The total force can then be calculated as the linear combination of the loads in each direction. The line loads are:

$$f_{FE} = \frac{F_N}{s_1 + s_2} \quad (3.3)$$

where s_1 and s_2 represent the half of the distance between the current node and the previous and following nodes along the launch vehicle IF ring. The percentage overflux is calculated as:

$$overflux = 100 \left(\frac{\max|f_{FE}|}{\max|f_{overall}|} - 1 \right) \quad (3.4)$$

It can be noted that when the overflux value is negative, the expected line loads are higher than the real ones, which is not a critical condition, whereas if the value is positive, the expected line loads are lower than the real ones, leading to a critical condition, especially for tensional loads.

3.3 Results

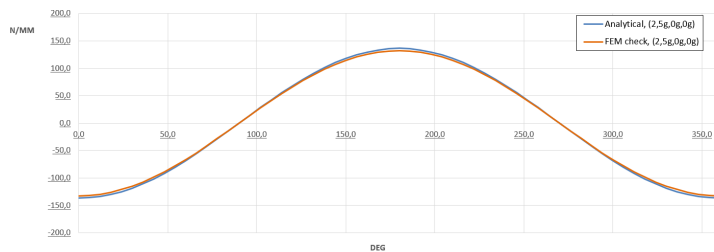
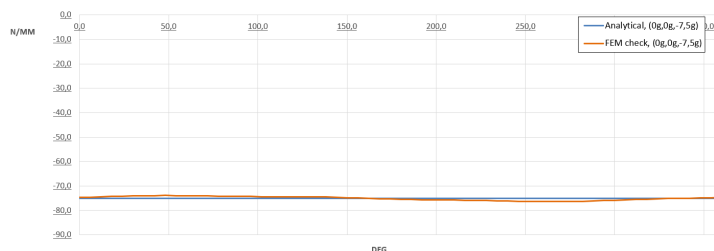
Tab. 3.1 shows the QSL values and their corresponding overfluxes. It can be noted how they never exceed the 10 % limit, and how for most of the cases they are negative. This happens because the spacecraft structure probably develops some local moments around the IF ring, therefore the M_{lat} is not balanced by just the F_N but also by such moments. Nevertheless all the resulting overfluxes are very close to zero, meaning that the real line loads are very well predicted by the analytical ones.

Table 3.1: Overflux computation

(a) $M_{lat} = M_y$			(b) $M_{lat} = M_x$		
QSL_{long} [g]	QSL_{lat} [g]	Overflux [%]	QSL_{long} [g]	QSL_{lat} [g]	Overflux [%]
-7.5	0	1.7	-7.5	0	1.7
-7.5	0.625	-1.4	-7.5	0.625	-1.8
-5	0.625	-1.6	-5	0.625	-2.0
-4.375	2.5	-2.5	-4.375	2.5	-2.7
0	2.5	-3.1	0	2.5	-3.2
1.875	2.5	-2.7	1.875	2.5	-2.7
1.875	0.625	-1.9	1.875	0.625	-1.5
2.5	0.625	-1.6	2.5	0.625	-1.2
2.5	0	1.7	2.5	0	1.7
2.5	-0.625	-2.0	2.5	-0.625	-2.4
1.875	-0.625	-2.2	1.875	-0.625	-2.5
1.875	-2.5	-2.8	1.875	-2.5	-3.0
0	-2.5	-3.1	0	-2.5	-3.2
-4.375	-2.5	-2.2	-4.375	-2.5	-2.1
-5	-0.625	-1.0	-5	-0.625	-0.3
-7.5	-0.625	-0.7	-7.5	-0.625	0.1

The signs of QSL_{long} were changed from the ones of the UM in order to be compliant with Nastran's sign convention, where a negative load is associated with compression. Another noteworthy observation is that for the same loading conditions but on different axis the results are somewhat different. This was expected as the spacecraft structure, although mainly symmetric, has some non-negligible asymmetries.

Figs. 3.2 and 3.3 show the fluxes in the cases of lowest and highest overflux value respectively.


 Figure 3.2: Fluxes for $QSL_{long} = 0$ and $QSL_{lat} = 2.5$; Overflux = -3.1 %

 Figure 3.3: Fluxes for $QSL_{long} = -7.5$ and $QSL_{lat} = 0$; Overflux = +1.7 %

3.4 Clamp band tension assessment

The clamp system usually adopted is the Marman clamp band, that keeps together the two axial-symmetric parts of the interface thanks to several V-shaped arch segments pressed towards a tightening belt on which the clamp band tension is applied by means of a screwed system and checked with load cells all along the circumference. An adequate clamp band tension is necessary in order to maintain SC and LV attached even in tensional loading conditions. Compressive loading is not a critical situation when analyzing the clamp band tension.

The minimum tension that has to be guaranteed is:

$$T_{min} = f_{max}^{radial} R_{IFSF} \quad \text{where : } f_{max}^{radial} = 2f_{max} \frac{\tan(\alpha) - \mu}{1 + \mu \tan(\alpha)} \quad (3.5)$$

$R_{IF} = 1.312$ is the radius of the interface, $\mu = 0.1$ is the friction coefficient between the surface of the SC and of the clamp, and $\alpha = 15$ is the angle described by the V-shape of the clamp. SF is a safety factor which was set to 2 as significant FoS should be applied to the calculated tightening force in order to account for possible overcoming excitation overshoots. f_{max} represents the maximum tensional line load reached during the mission, set accordingly to the previous static analysis and calculated with the analytical formulation, once confirmed that the discrepancies between analytic model and FEM are acceptable. Its values are shown in Tab. 3.2.

Table 3.2: Maximum tensional line loads

(a) $M_{lat} = M_y$			(b) $M_{lat} = M_x$		
QSL_{long} [g]	QSL_{lat} [g]	f_{max} [N/mm]	QSL_{long} [g]	QSL_{lat} [g]	f_{max} [N/mm]
-7.5	0	-76.39	-7.5	0	-73.56
-7.5	0.625	-107.73	-7.5	0.625	-43.15
-5	0.625	-17.9	-5	0.625	-17.87
-4.375	2.5	88.29	-4.375	2.5	87.51
0	2.5	132.28	0	2.5	132.06
1.875	2.5	151.13	1.875	2.5	151.16
1.875	0.625	51.92	1.875	0.625	52.11
2.5	0.625	58.21	2.5	0.625	58.47
2.5	0	25.46	2.5	0	25.46
2.5	-0.625	57.96	2.5	-0.625	57.77
1.875	-0.625	51.73	1.875	-0.625	51.59
1.875	-2.5	150.94	1.875	-2.5	150.65
0	-2.5	132.28	0	-2.5	132.09
-4.375	-2.5	88.71	-4.375	-2.5	88.77
-5	-0.625	-16.12	-5	-0.625	-16.32
-7.5	-0.625	-41.92	-7.5	-0.625	-41.83

The maximum tensional line load is then $f_{max} = 151.16 \text{ N/mm}$, which leads to $f_{max}^{radial} = 49.45 \text{ N/mm}$ and $T_{min} = 129.76 \text{ kN}$. Eq. 3.6 show the results of the lowest tension target in the case of one tightening bolt or two symmetrical tightening bolts respectively:

$$T_{min}^1 = T_{min} e^{\mu\pi} = 177.65 \text{ kN} \quad T_{min}^2 = T_{min} e^{\mu\frac{\pi}{2}} = 151.83 \text{ kN} \quad (3.6)$$

Chapter 4

Dynamic coupling

4.1 Process design

Once the mission is started, dynamic interactions between the launcher vehicle and the spacecraft are present, which can lead to the dynamic coupling of the two structures, connected at the interface. In order to study the dynamic coupling, a *lumped-parameter approach* was used in order to represent through a simplified model the behaviour of the dynamic interactions between SC and LV for different values of longitudinal frequency; furthermore, this model provides a clear explanation of the imposition of frequency requirements by the launcher authority. Lastly, it is well suited to represent really complex structures which can be represented through a reduced set of generalized coordinates, where each mode is related to a one DOF system.

4.2 Dynamic coupling model: Large Mass method

A generic 3 DOFs model is represented in Fig. 4.1a together with the model associated to the Falcon 9 in Fig. 4.1b:

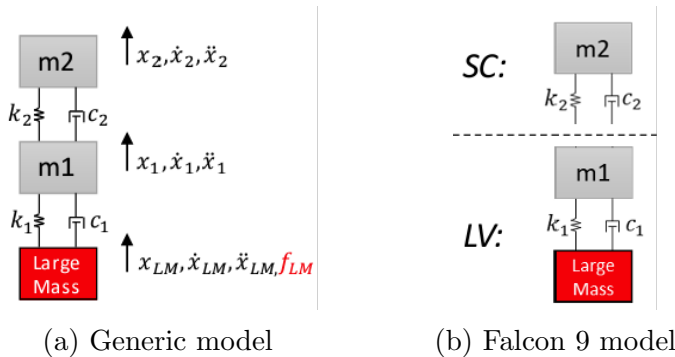


Figure 4.1: Simplified model of the Falcon 9's coupled system

The three DOFs are the displacements x_2 , x_1 and x_{LM} associated respectively to the SC (m_2), the LV (m_1) and an ideal LM (Large Mass). Each coordinate was taken with respect to an absolute reference such that the results could be directly retrieved. The *Large Mass method* implied prescribing an arbitrary acceleration to the DOF representing the base of the system, which is $LM = 10^6(m_2 + m_1)$; thus, the DOFs related to SC and LV were the only unknowns of the problem. The acceleration imposed on LM corresponds to the

acceleration applied on the vehicle by the engines.

The equations of motion of the system are reported in Eq. 4.1:

$$\begin{bmatrix} m_2 & 0 & 0 \\ 0 & m_1 & 0 \\ 0 & 0 & LM \end{bmatrix} \begin{Bmatrix} \ddot{x}_2 \\ \ddot{x}_1 \\ \ddot{x}_{LM} \end{Bmatrix} + \begin{bmatrix} c_2 & -c_2 & 0 \\ -c_2 & c_1 + c_2 & -c_1 \\ 0 & -c_1 & c_1 \end{bmatrix} \begin{Bmatrix} \dot{x}_2 \\ \dot{x}_1 \\ \dot{x}_{LM} \end{Bmatrix} + \begin{bmatrix} k_2 & -k_2 & 0 \\ -k_2 & k_1 + k_2 & -k_1 \\ 0 & -k_1 & k_1 \end{bmatrix} \begin{Bmatrix} x_2 \\ x_1 \\ x_{LM} \end{Bmatrix} = \begin{Bmatrix} 0 \\ 0 \\ F_{LM} \end{Bmatrix} \quad (4.1)$$

Where the parameters are:

$$k_i = m_i(2\pi f_i)^2 \quad (4.2)$$

$$c_{i,cr} = 2\sqrt{k_i m_i} \quad (4.3)$$

$$c_i = \xi c_{i,cr} \quad (4.4)$$

f_1 is the primary longitudinal frequency of the LV, F_{LM} is the force caused by the prescribed acceleration imposed to LM and $\xi = 0.05$ is a conventional value [2]. f_2 is the main longitudinal frequency of the SC and it is not a fixed value as it varies in a chosen range of values: this was done in order to study the dynamic coupling as the value of f_2 gets gradually closer to f_1 . It is expected that if f_2 is sufficiently far from f_1 , little to no dynamic coupling will arise and the acceleration on the base would not undergo to significant amplification in the spacecraft. On the other hand, if the frequency of the SC is close to the one of the LV, the acceleration on the base will be largely amplified on SC, and this can lead to catastrophic effects on the mission.

The hypothesis of sinusoidal solution and forcing was introduced:

$$\{x_i\} = \{X_i\} e^{j\omega t} \quad (4.5)$$

$$\{f_i\} = \{F_i\} e^{j\omega t} \quad (4.6)$$

X_i and F_i are respectively the complex amplitudes of the displacement and force, characterized by their own phase, and ω is the excitation frequency of the force. Introducing the hypothesis in Eq. 4.1 leads to:

$$(-\omega^2[m_{ii}] + \omega[c_{ii}] + [k_{ii}])\{X_i\} = \{F_i\} \quad (4.7)$$

Then the Frequency Response Function (FRF) amplitude displacement vector could be retrieved:

$$\{X_i\} = \text{inv}(-\omega^2[m_{ii}] + j\omega[c_{ii}] + [k_{ii}])\{F_i\} \quad (4.8)$$

Finally, the FRF amplitude acceleration vector was obtained:

$$\{\ddot{X}_i\} = -\omega^2\{X_i\} \quad (4.9)$$

It was then possible to study the transmissibility of the system, defined as:

$$T = \frac{|\ddot{x}_2|}{|\ddot{x}_{LM}|} \quad (4.10)$$

The value of T can be studied in order to observe the dynamic interactions between LV and SC. More specifically, three different situations can manifest:

- $T = 1$: the system is acting as a rigid body;
- $T > 1$: SC undergoes amplified accelerations (not desirable);
- $T < 1$: SC undergoes attenuated accelerations (desirable).

4.3 Results

The evolution of transmissibility for different spacecraft's longitudinal frequencies is displayed in Fig. 4.2 :

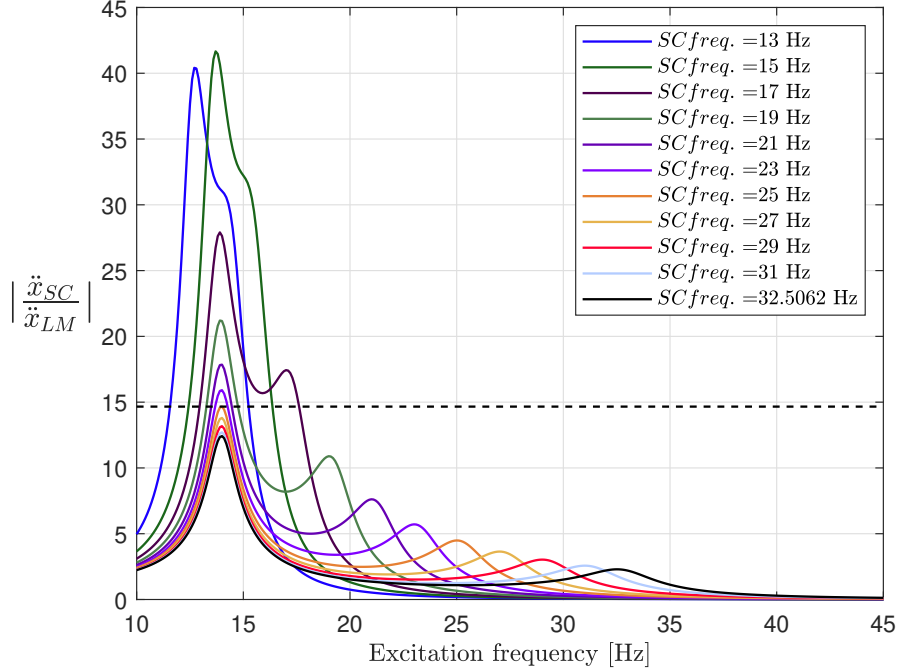


Figure 4.2: LV-SC dynamic coupling transmissibility

The range of the main longitudinal values of SC frequency goes from 31 to 13 Hz, having taken into account that $f_{LV}=14.1317$ Hz. Furthermore, the curve corresponding to $f_{SC}=32.5062$ Hz is included: this value of frequency is the primary mode of the spacecraft obtained through the modal analysis. The dashed line refers to the highest level of transmissibility reached by the curve associated to $f_{SC}=25$ Hz, which is the minimum value set by the user's manual. It is clear that, as the main longitudinal mode of SC decreases and approaches f_{LV} , the effects of the dynamic coupling become more significant; in particular, once the curve rises above the limit set by $f_{SC}=25$ Hz, the dynamic coupling effects grow quickly; it can be seen that, just by dropping the value of the frequency of SC from 25 to 15 Hz, the transmissibility level T grows from ~ 14 up to ~ 42 . Considering an harmonic acceleration of 1g imposed at the base, this would be amplified up to 42g at the spacecraft, and that would result in severe damage to the structure and to the payload.

To better understand the sensitivity of the problem and the relation between excitation frequency, SC frequency and transmissibility, a 3D plot containing the same information of Fig. 4.2 is displayed in Fig. 4.3:

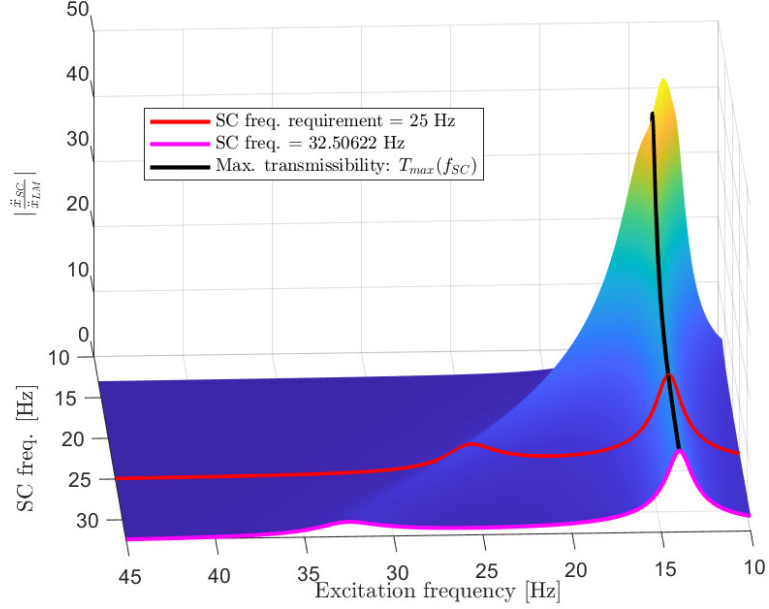


Figure 4.3: LV-SC dynamic coupling transmissibility

The curve of the maximum transmissibility $T_{max}(f_{SC})$ is portrayed in the $(T_{max}-f_{SC})$ plane in Fig. 4.4:

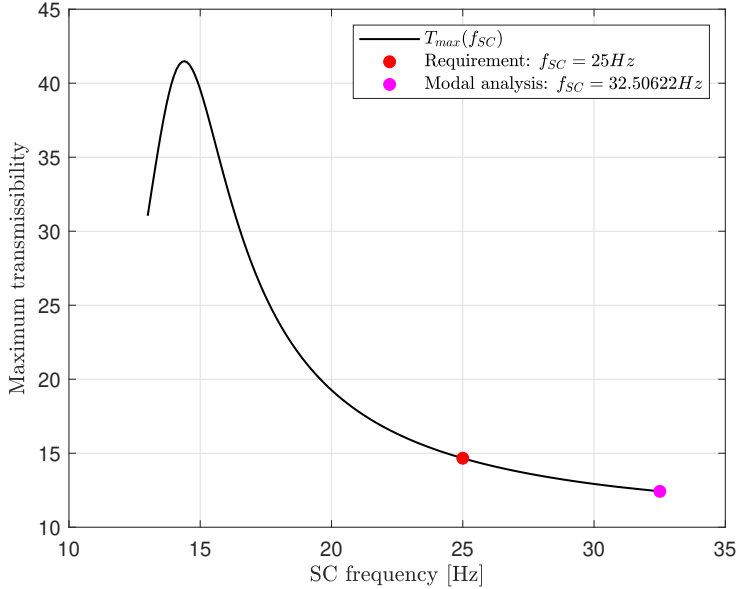


Figure 4.4: T_{max} evolution for different SC frequencies

The main longitudinal mode of the spacecraft meets the minimum requirement set by the user's manual; however, it can be noticed that the distance between the two values of frequency is not so relevant. This aspect implies that the transmissibility computed considering $f_{SC} = 32.50622$ Hz is slightly lower than the maximum value set by the requirement, as the curve tends to flatten. Therefore, if a decrease of T_{max} is required, it would be not so helpful to increment the main longitudinal mode's frequency value of the SC, as T_{max} would be minimally affected.

Chapter 5

Thermoelastic analysis

5.1 Introduction

By performing thermoelastic analysis, engineers can simulate and predict how the spacecraft's structure and components will respond to the different thermal loads that it may experience throughout its mission, enabling them to optimize the design, choose appropriate materials, and implement thermal control systems to mitigate potential issues arising from temperature variations in space. Usually, a several number of scenarios are studied in order to understand if the SC can fulfill all of its objectives along its activity, and if the structure and the payload can survive in different environments, too.

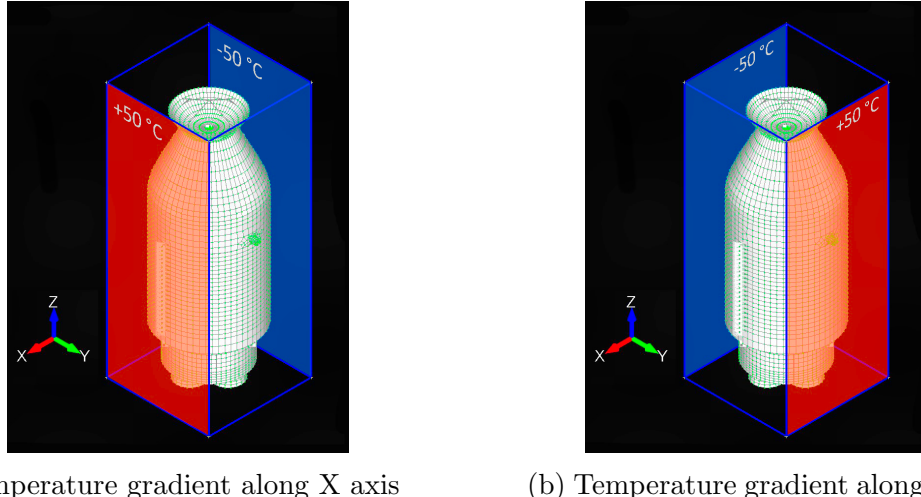
Now a particular scenario is studied: while in orbit, the telescope of the SC has to point towards a star exploiting the measurements given by the star trackers implemented in the spacecraft's set of sensors. The aim of the thermoelastic analysis is to compute the relative rotation between the star tracker and the telescope caused by the thermal deformation the spacecraft undergoes to. Starting from the hypothesis of perfectly (ideally) aligned bore-sights of star tracker and telescope in absence of thermoelastic influence, the results of this analysis shall be then taken into account for attitude control of the SC and for improving the pointing capability of the telescope even in presence of systematic errors introduced by the thermal conditions.

5.2 Thermoelastic model

For the analysis it was assumed that one side of the spacecraft is directed towards the Sun, while the other one is pointing towards deep space: this specific configuration generates a temperature gradient on the SC. To simulate this scenario, a parallelepiped enveloping the structure was created as shown in Fig. 5.1; the face corresponding to the side facing the Sun was kept at $+50\text{ }^{\circ}\text{C}$, while the face related to the opposite side was kept at $-50\text{ }^{\circ}\text{C}$. This is a simplified model, since in real application the thermal analysis is made directly on the surface of the SC. Since the implemented SC model is not perfectly symmetrical, two situations have been studied: in one case the normal vector of the two faces is aligned with the x axis, in the other one with the y axis. It is important to point out that a range of temperatures between $-50\text{ }^{\circ}\text{C}$ and $+50\text{ }^{\circ}\text{C}$ is not much representative of a real thermal load on the outer layers of the SC, where MLI (Multi Layer Insulation) is typically implemented, and in these regions temperatures can reach levels up to $100\text{-}200\text{ }^{\circ}\text{C}$. Since the MLI is not relevant from a structural point of view, it is neglected for the modeled structure; the temperatures taken into account stand for the temperatures on the plates

of the spacecraft.

To build the parallelepiped, a set of 80 thermal nodes is created, equally distributed in the four edges of the solid. This is a simplified model, since in real applications a number that range from 100 to 1000 nodes is typically included in the analysis. Nodes location and temperature are listed in Tab. 5.1 and Tab. 5.2.



(a) Temperature gradient along X axis

(b) Temperature gradient along Y axis

Figure 5.1: Thermoelastic model

$T = +50^\circ C$			$T = +50^\circ C$			$T = -50^\circ C$			$T = -50^\circ C$		
x [m]	y [m]	z [m]	x [m]	y [m]	z [m]	x [m]	y [m]	z [m]	x [m]	y [m]	z [m]
2.00	2.00	57.00	2.00	-2.00	57.00	-2.00	2.00	57.00	-2.00	-2.00	57.00
2.00	2.00	57.53	2.00	-2.00	57.53	-2.00	2.00	57.53	-2.00	-2.00	57.53
2.00	2.00	58.05	2.00	-2.00	58.05	-2.00	2.00	58.05	-2.00	-2.00	58.05
2.00	2.00	58.58	2.00	-2.00	58.58	-2.00	2.00	58.58	-2.00	-2.00	58.58
2.00	2.00	59.11	2.00	-2.00	59.11	-2.00	2.00	59.11	-2.00	-2.00	59.11
2.00	2.00	59.63	2.00	-2.00	59.63	-2.00	2.00	59.63	-2.00	-2.00	59.63
2.00	2.00	60.16	2.00	-2.00	60.16	-2.00	2.00	60.16	-2.00	-2.00	60.16
2.00	2.00	60.68	2.00	-2.00	60.68	-2.00	2.00	60.68	-2.00	-2.00	60.68
2.00	2.00	61.21	2.00	-2.00	61.21	-2.00	2.00	61.21	-2.00	-2.00	61.21
2.00	2.00	61.74	2.00	-2.00	61.74	-2.00	2.00	61.74	-2.00	-2.00	61.74
2.00	2.00	62.26	2.00	-2.00	62.26	-2.00	2.00	62.26	-2.00	-2.00	62.26
2.00	2.00	62.79	2.00	-2.00	62.79	-2.00	2.00	62.79	-2.00	-2.00	62.79
2.00	2.00	63.32	2.00	-2.00	63.32	-2.00	2.00	63.32	-2.00	-2.00	63.32
2.00	2.00	63.84	2.00	-2.00	63.84	-2.00	2.00	63.84	-2.00	-2.00	63.84
2.00	2.00	64.37	2.00	-2.00	64.37	-2.00	2.00	64.37	-2.00	-2.00	64.37
2.00	2.00	64.89	2.00	-2.00	64.89	-2.00	2.00	64.89	-2.00	-2.00	64.89
2.00	2.00	65.42	2.00	-2.00	65.42	-2.00	2.00	65.42	-2.00	-2.00	65.42
2.00	2.00	65.95	2.00	-2.00	65.95	-2.00	2.00	65.95	-2.00	-2.00	65.95
2.00	2.00	66.47	2.00	-2.00	66.47	-2.00	2.00	66.47	-2.00	-2.00	66.47
2.00	2.00	67.00	2.00	-2.00	67.00	-2.00	2.00	67.00	-2.00	-2.00	67.00

Table 5.1: Thermal nodes coordinates and temperatures for temperature gradient along X axis

$T = +50^\circ C$			$T = +50^\circ C$			$T = -50^\circ C$			$T = -50^\circ C$		
x [m]	y [m]	z [m]	x [m]	y [m]	z [m]	x [m]	y [m]	z [m]	x [m]	y [m]	z [m]
2.00	2.00	57.00	-2.00	2.00	57.00	2.00	-2.00	57.00	-2.00	-2.00	57.00
2.00	2.00	57.53	-2.00	2.00	57.53	2.00	-2.00	57.53	-2.00	-2.00	57.53
2.00	2.00	58.05	-2.00	2.00	58.05	2.00	-2.00	58.05	-2.00	-2.00	58.05
2.00	2.00	58.58	-2.00	2.00	58.58	2.00	-2.00	58.58	-2.00	-2.00	58.58
2.00	2.00	59.11	-2.00	2.00	59.11	2.00	-2.00	59.11	-2.00	-2.00	59.11
2.00	2.00	59.63	-2.00	2.00	59.63	2.00	-2.00	59.63	-2.00	-2.00	59.63
2.00	2.00	60.16	-2.00	2.00	60.16	2.00	-2.00	60.16	-2.00	-2.00	60.16
2.00	2.00	60.68	-2.00	2.00	60.68	2.00	-2.00	60.68	-2.00	-2.00	60.68
2.00	2.00	61.21	-2.00	2.00	61.21	2.00	-2.00	61.21	-2.00	-2.00	61.21
2.00	2.00	61.74	-2.00	2.00	61.74	2.00	-2.00	61.74	-2.00	-2.00	61.74
2.00	2.00	62.26	-2.00	2.00	62.26	2.00	-2.00	62.26	-2.00	-2.00	62.26
2.00	2.00	62.79	-2.00	2.00	62.79	2.00	-2.00	62.79	-2.00	-2.00	62.79
2.00	2.00	63.32	-2.00	2.00	63.32	2.00	-2.00	63.32	-2.00	-2.00	63.32
2.00	2.00	63.84	-2.00	2.00	63.84	2.00	-2.00	63.84	-2.00	-2.00	63.84
2.00	2.00	64.37	-2.00	2.00	64.37	2.00	-2.00	64.37	-2.00	-2.00	64.37
2.00	2.00	64.89	-2.00	2.00	64.89	2.00	-2.00	64.89	-2.00	-2.00	64.89
2.00	2.00	65.42	-2.00	2.00	65.42	2.00	-2.00	65.42	-2.00	-2.00	65.42
2.00	2.00	65.95	-2.00	2.00	65.95	2.00	-2.00	65.95	-2.00	-2.00	65.95
2.00	2.00	66.47	-2.00	2.00	66.47	2.00	-2.00	66.47	-2.00	-2.00	66.47
2.00	2.00	67.00	-2.00	2.00	67.00	2.00	-2.00	67.00	-2.00	-2.00	67.00

Table 5.2: Thermal nodes coordinates and temperatures for temperature gradient along Y axis

Each node is set to influence at most 30% of the structure and each temperature value is interpolated through the two closest nodes.

The CTEs (Coefficient of Thermal Expansion) and the reference temperature of the materials of the spacecraft are reported in Tab. 5.3. The thermoelastic deformation is expressed as:

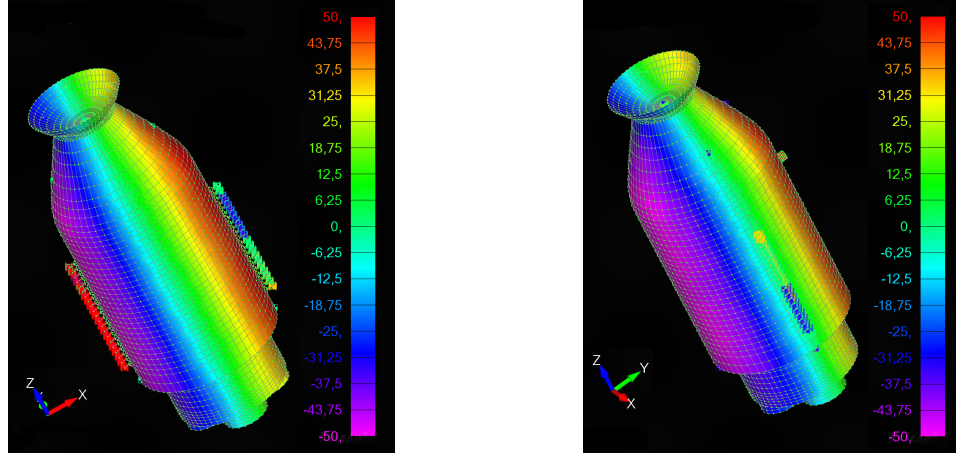
$$\Delta l = \alpha \Delta T l_0 \quad (5.1)$$

where Δl is the deformation, α is the CTE, $\Delta T = T - T_{ref}$ and l_0 is the initial length.

Subsystem	CTE [$\frac{1}{^\circ C}$]	Ref. temperature [$^\circ C$]
Main structure	8.5E-6	22.5
Engine enforcing plate	3E-6	22.5
Engine and tanks	8.5E-6	22.5
Cover	2.3E-5	22.5
Telescope	2.3E-5	22.5
Stiffer beams	8.5E-6	22.5
Weaker beams	2.3E-5	22.5

Table 5.3: SC's coefficients of thermal expansion

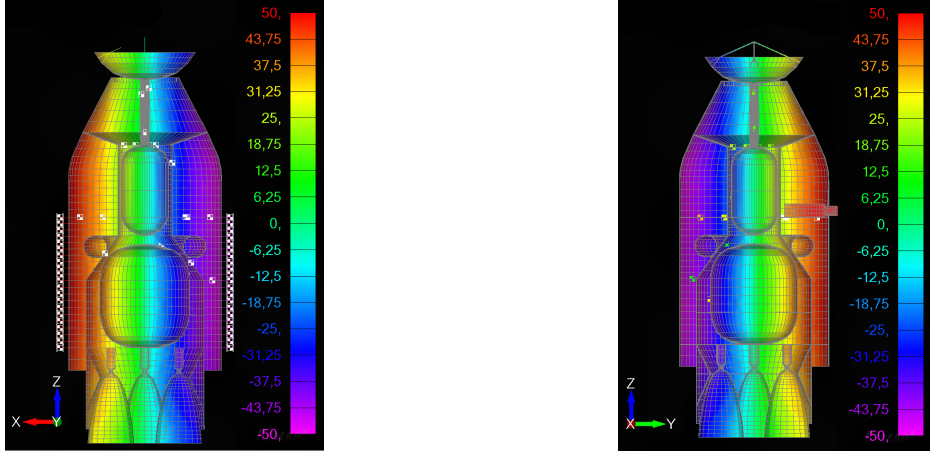
The thermal maps of the SC are portrayed in Fig. 5.2. It is clear that in both cases, the thermal gradient does not show any substantial difference in its behaviour.



(a) Temperature gradient along X axis

(b) Temperature gradient along Y axis

Figure 5.2: Thermal map of SC



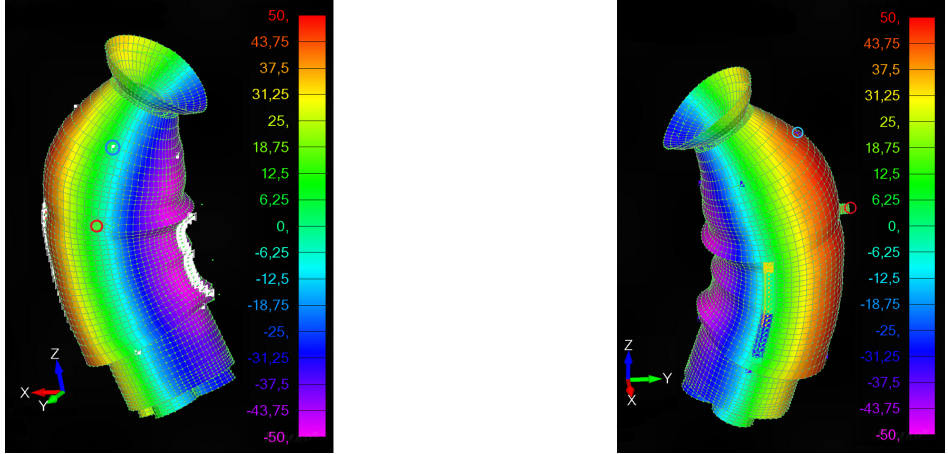
(a) Temperature gradient along X axis

(b) Temperature gradient along Y axis

Figure 5.3: Thermal map of SC's inner components

5.3 Results

The solution of the thermoelastic analysis is obtained through MSC Nastran through **template 101-Static-Thermoelastic run.dat** code. Before delving into the analysis, it's crucial to address the applied boundary conditions. Since the thermoelastic analysis is centered around depicting the satellite in orbit, constraining the nodes of the SC interface would not make sense. However, in a static analysis, the absence of constraints would render the stiffness matrix singular, triggering a fatal error. To tackle this issue, a different form of constraint is implemented for this analysis: leveraging the structure's inertia to constrain its Center of Gravity (COG) using the MSC Nastran command **PARAM, INREL,-2** [3]. This approach aims to immobilize the structure's COG both in translation and rotation, which essentially mimics the impact of a thermoelastic deformation while conserving momentum. The outputs of the analysis are displayed in Fig. 5.4:



(a) Temperature gradient along X axis (b) Temperature gradient along Y axis

Figure 5.4: Deformation due to thermoelastic effects

As mentioned earlier, the aim of this analysis is to compute the relative rotation between the telescope (red circled) and one of the star trackers (blue circled).

Table 5.4: Absolute rotations

(a) Temperature gradient along X axis			(b) Temperature gradient along Y axis			
Unit	$\ \theta_x\ [^\circ]$	$\ \theta_y\ [^\circ]$	Unit	$\ \theta_x\ [^\circ]$	$\ \theta_y\ [^\circ]$	
Telescope	0.0214	0.0523	0.0614	Telescope	0.0212	3.0145E-7
Star tracker	0.0254	0.1435	0.0650	Star tracker	0.1385	4.2158E-5

Table 5.5: Relative rotations

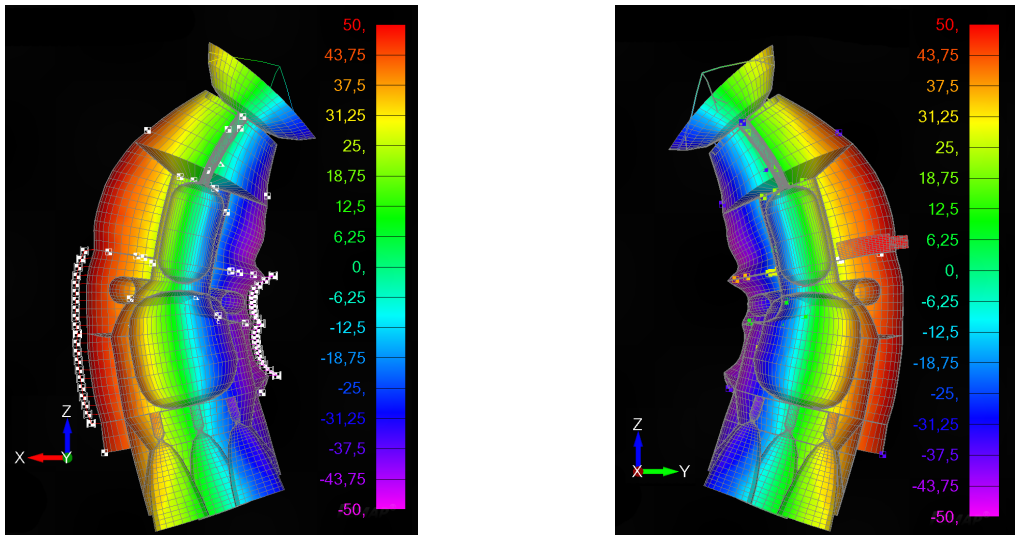
(a) Temperature gradient along X axis			(b) Temperature gradient along Y axis		
$\ \theta_x^r\ [^\circ]$	$\ \theta_y^r\ [^\circ]$	$\ \theta_z^r\ [^\circ]$	$\ \theta_x^r\ [^\circ]$	$\ \theta_y^r\ [^\circ]$	$\ \theta_z^r\ [^\circ]$
0.0040	0.0912	0.0036	0.1172	4.1857E-5	9.6406E-5

It can be noticed how, in Tab. 5.5, the relative rotations between the two components change by orders of magnitude depending on the direction of the temperature gradient: the reason is that the sensor chosen for the analysis and the telescope are located on the side associated to the face of the parallelepiped which is pointing in the +Y direction. Indeed, in Tab. 5.5b the rotations $\|\theta_y^r\|$ and $\|\theta_z^r\|$ are in the order of 10^{-5} : considering that usually the accuracy of a star tracker is in the order of 1 arcsecond [4], these values are acceptable. The same can not be said for $\|\theta_x^r\|$ which is in the order of 10^{-1} : such a rotation is extremely high with respect to the typical performances regarding pointing requirements for the pointing of a telescope. Regarding the values reported in Tab. 5.5a, every relative rotation is higher than the standard performance of pointing a star tracker should be able to provide: $\|\theta_x^r\|$ and $\|\theta_z^r\|$ are in the order of 10^{-3} , which is higher than 1 arcsecond, and $\|\theta_y^r\|$ reaches the order of 10^{-2} . These rotations, as well as $\|\theta_x^r\|$ in Tab. 5.5b are not negligible and would result in a poor quality pointing by the telescope. Furthermore, these errors can easily propagate and have significant effects on other quantities; so, even if they are known and corrected a posteriori, the best thing to do is to

reduce these values of relative rotation in the successive iterations of the design process of the spacecraft.

An approach that aims to improve the design could involve the modification of structural materials to decrease the CTE. In this preliminary evaluation, some materials are characterized by a relatively high value of this coefficient; an alternative choice of the materials can take into consideration composite materials because of their lower or even negative CTE. It's important to note that the detected high rotation in this initial analysis doesn't necessarily denote a drawback: these obtained outputs are remarkably informative and can significantly guide the subsequent iterations of SC design. When progressing to a real-world scenario, it's crucial to emphasize and communicate these results effectively to steer the troubleshooting process accurately. Additionally, ensuring positive safety margins within the structure becomes imperative at this point of the process.

Finally, the deformation caused by the thermal loads of the inner components of the spacecraft is displayed in Fig. 5.5 :



(a) Temperature gradient along X axis

(b) Temperature gradient along Y axis

Figure 5.5: Deformation of the inner components due to thermoelastic effects

Chapter 6

Sine testing

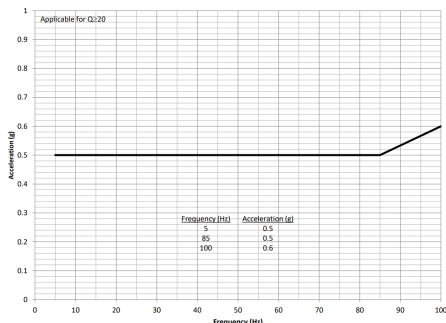
6.1 Process design

The goal of the sine vibration test is to validate the spacecraft's structural integrity when subjected to the maximum flight loads, adjusted by the necessary safety margin. The sine test aims to simulate the intensity of transient conditions at the LV-SC interface with a conservative sine environment. The designated frequency spectrum for the Falcon 9 launcher spans from 5 to 100 Hz, commonly denoted as the low-frequency range. In sine vibration test, the IUT (Item Under Test) is fixed on a table, and a base acceleration is imposed by moving the table with an electrodynamic (or hydraulic) shaker. Three separate mono-axial excitation runs are performed enforcing an acceleration which respects a sine sweep function. The frequency of the sine progressively increases with time [2]:

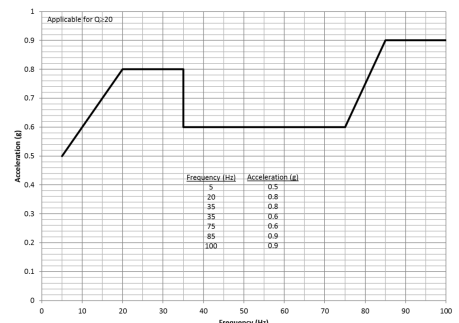
$$a_{sw}(t) = \sin \left(2\pi \frac{60f_0}{K_e \ln(2)} \left(2^{(K_e/60)t} - 1 \right) \right) \quad (6.1)$$

where $f_0 = 2\pi\omega_0$ (with $\omega_0 = 5 \text{ Hz}$) is the starting circular frequency of the sweep and $K_e = 2 \text{ oct/min}$ is the sine sweep rate [1]. The sine test represents the most severe mechanical test the spacecraft undergoes, demanding a conservative approach to guarantee its ability to withstand the loads. During the design phase, the sine test is numerically simulated using the sine test prediction to validate the actual test's safety with sufficient margins. The qualification levels of the excitation to be imposed to the LV-SC interface are indicated in the LV UM, and are shown in Fig. 6.1 and they don't include a safety margin, which will be applied later.

Figure 6.1: Sinusoidal vibration levels for a single launch configuration [1]



(a) Maximum limit level lateral equivalent sine environment for Falcon 9



(b) Maximum limit level axial equivalent sine environment for Falcon 9

6.2 Primary notching

The definition of notching is “a Test excitation spectrum reduction, occurring in a specific frequency range, operated in order to keep the response of a location of interest of the test item under a specified amplitude (e.g. in the proximity of a resonant frequency)” [2]. So a reduction in the sine test input profile for a certain frequency range is necessary to protect the structures from over testing. The lateral moments obtained during the sine tests along the X and Y-axis and the axial force obtained during the z-axis test, have to remain below the corresponding limit levels calculated as in eq. 3.1. The results are shown in Tab. 6.1.

Table 6.1: Limits on the lateral moments and axial force

M_y [daNm]	M_x [daNm]	F_z [daN]
75247	75247	63126

6.3 Secondary notching

It may be necessary to notch again the sine test profile, this time to protect the on-board equipment. Indeed, each instrument is qualified up to a certain level of maximal acceleration, and if the excitation of the Payload (PL) during the sine test prediction surpasses its qualified limit, a consensus with the launcher authority must be reached to adjust the sine test input profile. The antenna’s qualification levels are shown in Tab 6.2. There is a threshold on this reduction: the secondary notched sine test input profile shall be greater than the ESI (Equivalent Sine Input) curve in order to respect the launcher authority regulations. Indeed, the ESI limitation cannot be violated not to jeopardize the conservativeness of the test and to avoid the risk of undertest with respect to the severity of the mission loads.

Table 6.2: Antenna qualification levels

Lateral qualification level [g]	Axial qualification level [g]
10	25

6.4 ESI

The ESI represents the harmonic sine input (experienced during the shaker test) that is equivalent to a transient excitation (experienced during the flight) of a 1DOF system. In order to compute the ESI, first of all it is necessary to simulate a transient time history of the acceleration at the IF (Interface) during the flight with the CLA (Coupled Load Analysis). This was done considering an equivalent 1DOF spring, mass and damper system of the SC, where the mass corresponds to m_{SC} and each 1DOF system is characterized by a different stiffness and consequently by a different resonance frequency $\omega = \sqrt{\frac{k}{m}}$. Then the Shock Response Spectrum (SRS) curve was calculated recovering the maximum absolute value of the response (acceleration \ddot{x}) for each 1DOF system natural frequency

from 5 to 100 Hz. Lastly, the ESI was obtained dividing the SRS by $Q = \frac{1}{2\xi}$, the quality factor, where ξ is the modal damping ratio. In this case, since $\xi = 0.02$, then $Q = 25$.

6.5 Results

The model used to run the following analysis is the one including spacecraft and third stage of the LV. Two rigid elements were created, one connecting the ring nodes of the SC - LV interface to a master node at the center of the IF, and one connecting the nodes of the nozzle to a master node at its center. For the sine testing a set of 6 very stiff springs (one for each DOF) was added connecting the IF central node to another node in the same position. These springs are not present while running the transient analysis.

The sine test prediction was performed with MSC Nastran (**111 solution sequence code** for the Modal Frequency Response) one axis per time considering a unitary FRA (Frequency Response Analysis). Then, exploiting the linearity of the problem, the results were multiplied by the correction factor of the sine test input profile (Fig. 6.1). As expected, around the resonant frequency both the lateral moments and the longitudinal force have a peak, therefore at those frequencies primary notching was applied. Considering the payload accelerations, in all of the three tests they peak at a much higher value than the limit for which the PL is qualified. Thus, secondary notching is always required. It is important to notice how in neither case the secondary notching has to be applied at the same frequencies in which primary notching is present, nor the secondary notched profile goes below the ESI.

The ESI was calculated as explained in 6.4 starting from a modal transient analysis in MSC Nastran (**112 solution sequence code** for the Modal Transient Response) considering the forces shown in Fig. 6.2 applied to the center of the nozzle of the LV 3rd stage.

Figure 6.2: Input forces for the CLA

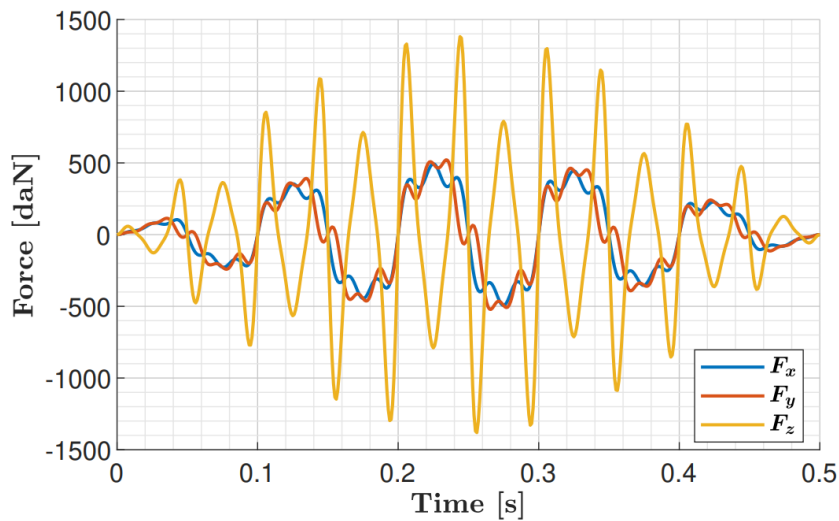
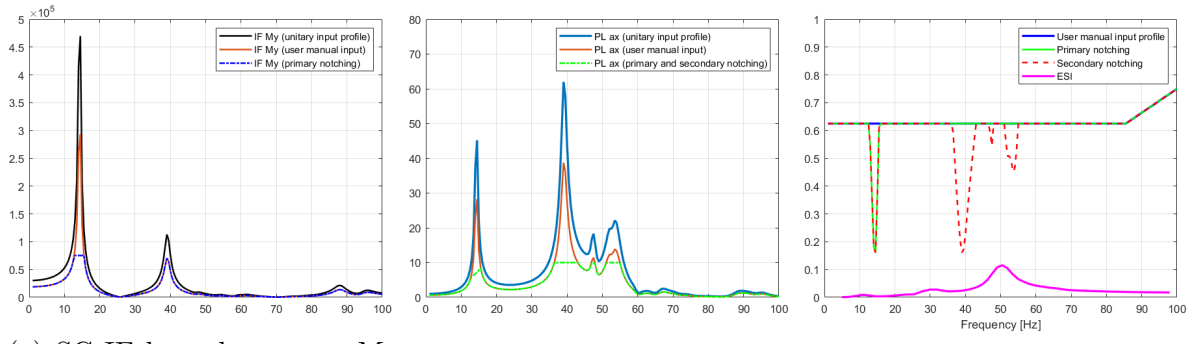
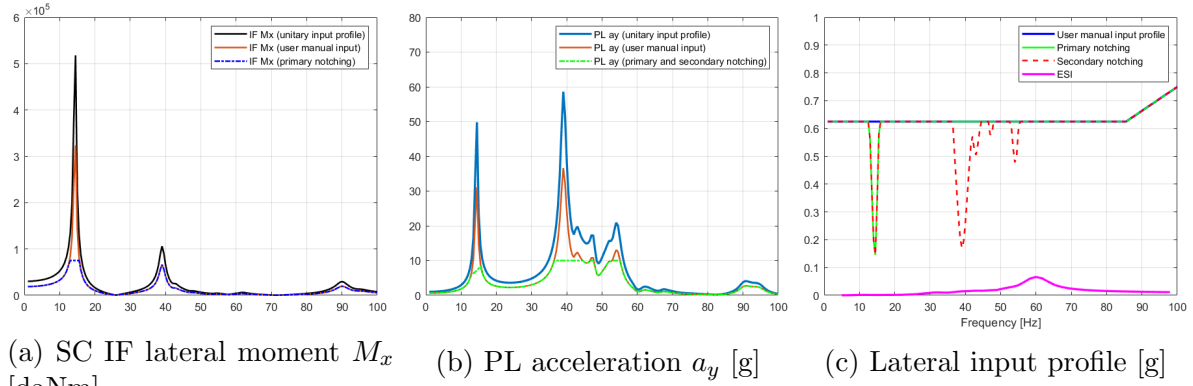


Figure 6.3: Sine X test prediction results



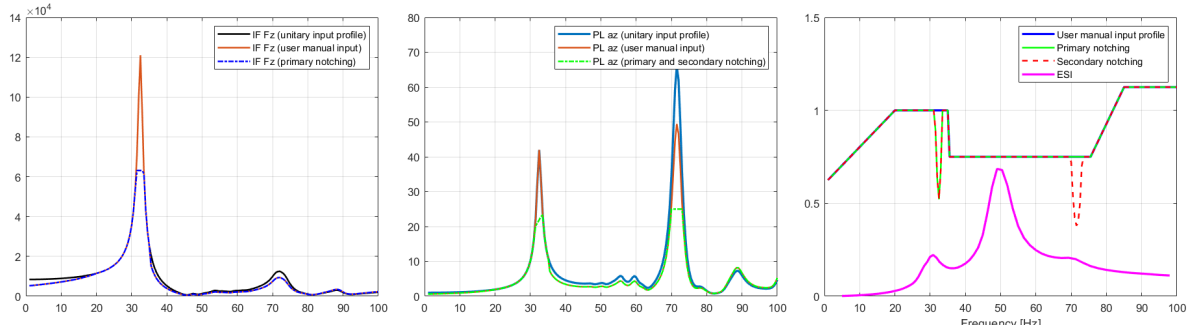
(a) SC IF lateral moment M_y [daNm] (b) PL acceleration a_x [g] (c) Lateral input profile [g]

Figure 6.4: Sine Y test prediction results



(a) SC IF lateral moment M_x [daNm] (b) PL acceleration a_y [g] (c) Lateral input profile [g]

Figure 6.5: Sine Z test prediction results



(a) SC IF axial force F_z [daN] (b) PL acceleration a_z [g] (c) Axial input profile [g]

Chapter 7

Acoustic testing

7.1 Introduction

Once the analysis of the spacecraft response to the lower frequency excitation was done the next step was to study the response of a specific unit to the acoustic qualification test environment. As in sine testing the spacecraft is tested on the shaker but this test involves random loads to represent the acoustic perturbations. On the shaker the space structure was excited on each of the three axis individually: it is not really consistent to the flight environment but in this way we are even more conservative. The Falcon 9 launcher user's manual declares the maximum sound pressure levels during the flight for both Cape Canaveral and Vanderberg launch sites as a function of frequency in third-octave or full octave, expressed in dB. The table in third-octave for the launch from Vanderberg site is shown on the right. In this table the available frequencies are up to 10000 Hz. However, for an acoustic test analysis, we are mostly interested in the frequency range up to 2000 Hz because in acoustic loads the majority of energy is concentrated below this value. The formula to express the sound pressure level in dB is the following:

$$SPL_{dB} = 10 \log_{10} \frac{P_{RMS}^2}{P_{ref}^2} = 20 \log_{10} \frac{P_{RMS}}{P_{ref}} \quad (7.1)$$

where P_{RMS} is the root mean square of the sound pressure, and its meaning is to represent a random phenomenon as an average value. The P_{ref} value is a reference point, meant to represent the lowest value of pressure that can be sensed by the human ear, and is conventionally set to $2 \times 10^{-5} Pa$. The reason for the elevation of the two pressure terms to the power of two is that we are interested in representing the energetic content of that pressure field, which is always a quadratic term. Since the SPL is given by the launcher user manual, the root mean square of the pressure elevated to the power of two can be retrieved by inverting the previous equation.

Frequency [Hz]	SPL [dB]
31,5	119,75
40	120
50	120
63	120
80	119,8
100	120,5
125	121,5
160	122
200	121,5
250	120,5
315	119
400	117
500	115
630	113
800	111
1000	109,5
1250	108
1600	107
2000	106
2500	105
3150	104
4000	103
5000	102
6300	101
8000	100
10000	99

Table 7.1: Acoustic vibration qualification level

$$P_{RMS}^2 = P_{ref}^2 10^{\frac{SPL_{dB}}{10}} \quad (7.2)$$

This new parameter can be converted into the Pressure Power Spectral Density *PPSD* by dividing it with the relative frequency band (eq. 7.3) where the latter can be expressed in a more convenient way, see eq. 7.4.

$$PPSD = \frac{P_{RMS}^2}{\Delta f} \quad (7.3)$$

$$\Delta f = f_2 - f_1 = (2^{1.6} - 2^{-1.6})f_c = 0.2316 * f_c \quad (7.4)$$

This last equation is referred to the 1/3 octave logarithmic scale and f_c is the relative frequency in Tab. 7.1, representing the center of the bandwidth. The PPSD is the actual input of Nastran simulation for this analysis while the output of the simulation is an acceleration power spectral density (APSD). Once the PPSD was calculated for each frequency range, a useful operation that could be undertaken is to divide the result by the square of the gravitational acceleration. Since the unit measures of the original PPSD and the output of Nastran are Pa^2/Hz and $(\frac{m}{s^2})/Hz$, the reason for this last operation is to extract as output from Nastran an acceleration which is expressed in g accelerations, as it was done in the previous analysis. The final result, the PPSD expressed in $Pa^2/(g^2 Hz)$, is the mechanical pressure load that is imposed on the panels of the spacecraft model during the Nastran simulation. Although it is supposed to be applied only on the external panels, for this analysis all the plates of the model are subjected to it, in order to be more conservative.

All the quantities above, calculated for each frequency band from Tab. 7.1, can be found in Tab. 7.2 below:

Frequency [Hz]	SPL [dB]	Δf [Hz]	P_{RMS}^2	P_{RMS}	$PPSD$	$PPSD/g^2$
31,5	119,75	7,30	377,62	19,432	51,761	0,537864
40	120	9,26	400	20	43,178	0,448666
50	120	11,58	400	20	34,542	0,358933
63	120	14,59	400	20	27,415	0,284867
80	119,8	18,53	381,99	19,545	20,617	0,214236
100	120,5	23,16	448,81	21,185	19,379	0,201365
125	121,5	28,95	565,02	23,770	19,517	0,202803
160	122	37,06	633,96	25,176	17,108	0,177772
200	121,5	46,32	565,02	23,770	12,198	0,126752
250	120,5	57,90	448,81	21,185	7,7512	0,080546
315	119	72,95	317,73	17,825	4,3554	0,045256
400	117	92,64	200,47	14,159	2,1643	0,022487
500	115	115,80	126,4	11,247	1,0923	0,011350
630	113	145,91	79,81	8,934	0,5470	0,005684
800	111	185,28	50,36	7,096	0,2718	0,002824
1000	109,5	231,60	35,65	5,971	0,1539	0,001599
1250	108	289,50	25,24	5,024	0,0872	0,000906
1600	107	370,56	20,05	4,477	0,0541	0,000562
2000	106	463,20	15,92	3,990	0,0344	0,000357
2500	105	579	12,65	3,557	0,02185	0,000227
3150	104	729,54	10,05	3,169	0,01377	0,000143
4000	103	926,4	7,981	2,825	0,00862	0,000090
5000	102	1158	6,339	2,518	0,0055	0,000057
6300	101	1459,08	5,036	2,244	0,0035	0,000036
8000	100	1852,8	4	2	0,0022	0,000022
10000	99	2316	3,177	1,783	0,00137	0,000014

Table 7.2: Nastran input computation

From the available data it is possible to retrieve another useful quantity which is the Over-All Sound Pressure Level (OASPL), using the following formula:

$$OASPL = 10\log_{10}\left(\sum_{i=1}^n 10^{\frac{SPL(i)}{10}}\right) = 131.3775 \quad (7.5)$$

where n is number of rows in Tab. 7.2. To be noted that the OASPL result in 7.5 is in accordance with the value communicated in the launcher user manual.

7.2 Qualification standards

The goal of the Nastran simulation is to retrieve the expected response and in particular a quantity representing the maximum acceleration of one of the equipment components on the spacecraft, in this case the telescope, due to the mechanical load generated by the random vibration of the panel to which it is attached to. The output of the simulation, the APSD, has then to be compared to the value coming from the qualification standard level of the unit, in order to be sure that the component will not break during the real acoustic random test, and thus during the launch. For this the NASA Goddard Space Flight Center General Environmental Verification Standard (GSFC) was taken as a reference. Here the maximum allowed accelerations expressed by the standard is also a function of the payload mass, not only of frequency, see Fig. 7.1 below:

Generalized Random Vibration Test Levels Components (ELV) 22.7-kg (50-lb) or less		
Frequency (Hz)	ASD Level (g^2/Hz)	
	Qualification	Acceptance
20	0.026	0.013
20-50	+6 dB/oct	+6 dB/oct
50-800	0.16	0.08
800-2000	-6 dB/oct	-6 dB/oct
2000	0.026	0.013
Overall	14.1 G _{rms}	10.0 G _{rms}

The acceleration spectral density level may be reduced for components weighing more than 22.7-kg (50 lb) according to:

	Weight in kg	Weight in lb	
dB reduction	= 10 log(W/22.7)	10 log(W/50)	
ASD(50-800 Hz)	= 0.16•(22.7/W)	0.16•(50/W)	for protoflight
ASD(50-800 Hz)	= 0.08•(22.7/W)	0.08•(50/W)	for acceptance

Where W = component weight.

The slopes shall be maintained at + and - 6dB/oct for components weighing up to 59-kg (130-lb). Above that weight, the slopes shall be adjusted to maintain an ASD level of 0.01 g²/Hz at 20 and 2000 Hz.

For components weighing over 182-kg (400-lb), the test specification will be maintained at the level for 182-kg (400 pounds).

Figure 7.1: GSFC standard, [5]

The mass of the telescope is 63,60 kg, thus higher than the 22.7 kg value to which Fig. 7.1 is referring. At the bottom of the table the rules for determining the maximum acceleration spectral density level for each frequency is specified for higher values of unit mass. In our case the maximum ASD level of $0.01 \text{ g}^2/\text{Hz}$ should be fixed for 20 and 2000 Hz, while the slopes of the lateral curves should be chosen in order to respect the APSD value in the flat portion given by the following expression:

$$ASD_{50 < f < 800} = 0.16 \frac{22.7}{W} = 0.0571 \quad (7.6)$$

For the first portion of the curve, since both initial and final points are fixed, the expression for the slope is shown in eq. 7.7:

$$SLOPE_{dB} = \frac{10 \log_{10}(\frac{ASD_2}{ASD_1})}{\log_2 \frac{f_2}{f_1}} = 5.724 \frac{dB}{oct} \quad (7.7)$$

The same equation 7.7 leads to the second slope value equal to $-5.724 \frac{dB}{oct}$. By using the just computed results it is possible to invert the equation in order to retrieve the APSD values at the two ends of the interval of interest:

$$APSD_0 = PSD_2 10^{-\frac{SLOPE_1 \log_2(\frac{f_2}{f_0})}{10}} = 2.677 \times 10^{-3} \quad (7.8)$$

$$APSD_4 = PSD_3 10^{-\frac{SLOPE_2 \log_2(\frac{f_3}{f_0})}{10}} = 4.687 \times 10^{-4} \quad (7.9)$$

where f_2 and f_3 are respectively 50 and 800 Hz. This last operation is optional, since the qualification levels are expressed only for 20-2000 Hz range.

7.3 Process design

As already stated the chosen component to be analysed is the telescope, once again. Inside the structure of the spacecraft it was constrained simultaneously by the internal horizontal surface, which is meant to sustain the majority of payload and actuators, and by the external panel, in correspondence of its upper part. During the analysis the output will be recorded at the node located at the tip of the telescope, on its axis. To run the modal frequency response of the spacecraft the following inputs were given to Nastran:

- the mesh of the spacecraft;
- the location of the reference node of the telescope;
- the PPSD retrieved from the launcher user manual, as a function frequency, which was applied to all surface elements of the mesh;
- the list of nodes at the adapter interface with the relative rigid constraint;
- the damping of the system as a function of frequency;
- the frequency range in which the response has to be calculated, which is coincident with the range of frequencies in which the SPL was declared.
- The range of frequencies in which the Lanczos solver must search the resonance frequencies for the modal response.

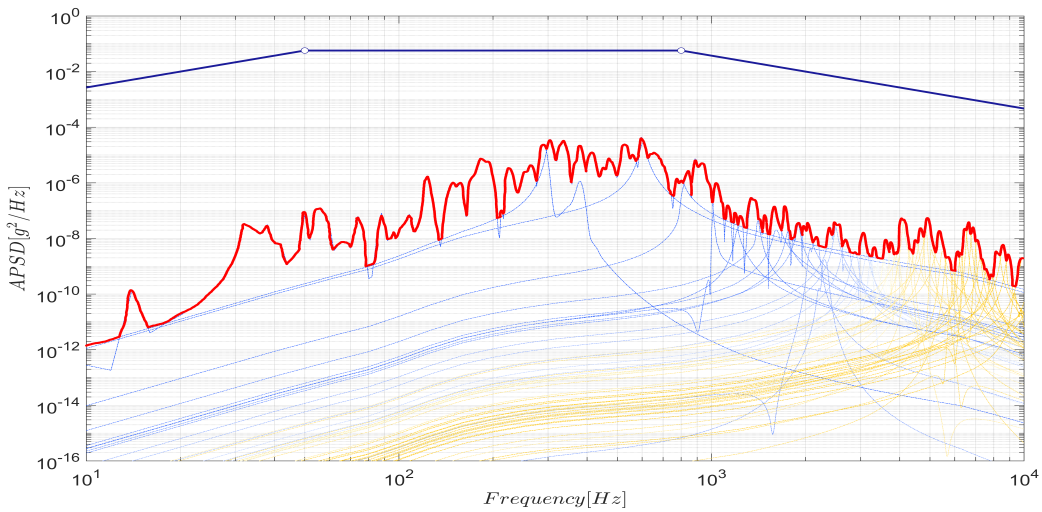
This last element of the list ideally should envelop the entire range of frequencies in which the acoustic perturbation is considered, up to 10000 Hz. For example a convenient upper limit for this range would be 12000 Hz. The reason for this is to make sure that also the modal response relative to the frequencies right after the 10000 are considered, since a major resonance peak could appear in that position. The modes whose frequencies are much higher than our range of interest will not contribute significantly on the response of the system. Because of the very high computational demand required by the simulation, it was not possible to cover the entire 12000 Hz range by running a unique simulation, hence Nastran was not giving any output for frequency range amplitudes above 200 Hz. Thus the analysis was subdivided into many simulations with short frequency range, which was progressively enlarged up to 800 Hz when the density of modal frequencies seemed to decrease, and shortened in the opposite case. When the last simulation was completed and the output was saved, the final result of the analysis was computed by considering for each frequency the highest amplitude from all the contributions, which are functions of frequency. To do this the vectors containing the APSD values needed first to be interpolated along a common frequency vector because depending on the modal density of its relative frequency range, each individual response output presented a different number of vector components.

This process could be done because, since the analysis is a modal response to a perturbation, its complete result can be approximated by the overlapping of all the contributions represented by the modes of the dynamic system.

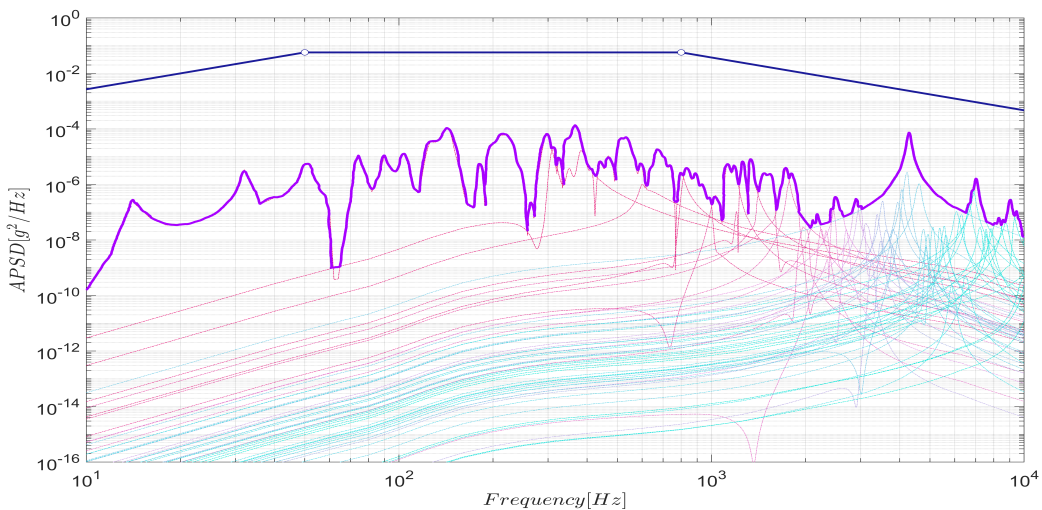
7.4 Results

In Fig. 7.2, it is possible to observe the result of the random acoustic test prediction along the three axis. The blue line represents the sum of all the individual simulations which were done to cover the entire 12000 Hz frequency range, which are represented by the colored curves. In order to better distinguish the responses between the ones associated to higher and lower frequency modes, to each line a different color was associated, creating in such a way a color gradient.

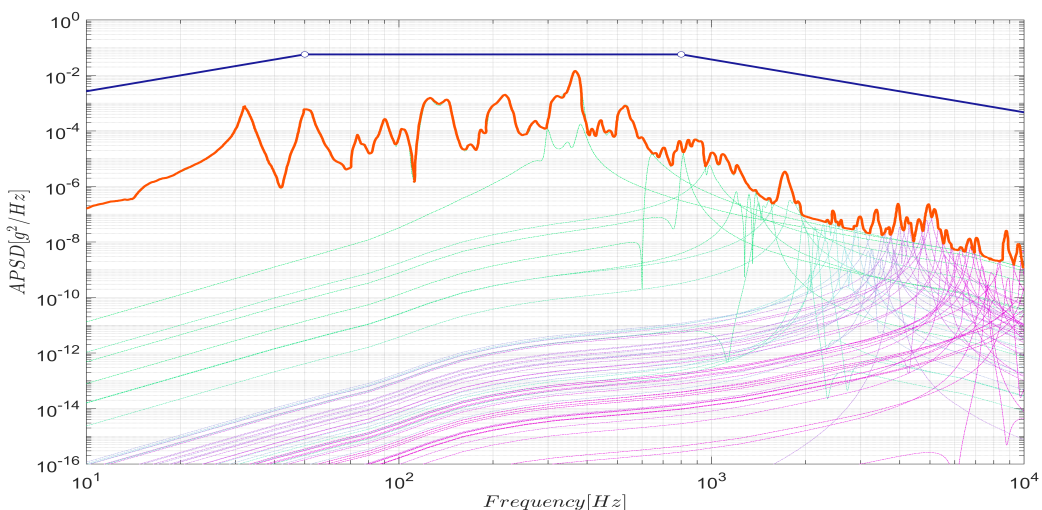
On the same charts the qualification APSD level was plotted in order to compare the Nastran output with it. It is clear that the APSD prediction is completely enveloped by the qualification standard level, leading to the assurance that the component inside the spacecraft will resist to the random solicitation during the test on the shaker, and during the flight. There are two peaks of the APSD result which mostly approach the qualification level, one in the chart referred to the Z axis, which is the most critical along the three, and one in the chart referred to the Y axis, at 4000 Hz. However, regarding the second case, although the qualification APSD was plotted along the entire frequency range, we are mostly interested in the frequencies which are not exceeding 2000 Hz because the higher frequencies should be covered by the shock analysis.



(a) *Xaxis*



(b) *Yaxis*



(c) *Zaxis*

Figure 7.2: Acceleration power spectral density

Chapter 8

Severity Comparison

In the previous chapter a comparison between the Acceleration PSD coming from the simulation and the one from the qualification standard of the unit was done, leading to a satisfying conclusion. However the APSD is not properly a representative of the severity of a load, expressed in g accelerations, but it is a spectral density. In order to come to a more realistic conclusion the two APSD curves must be converted into a new function of the frequency, the severity spectrum curve, which expresses the highest expected acceleration of a mass in a one DOF system, when it is subjected to its own resonance frequency. This single DOF system is characterized by a certain damping, which conventionally is fixed by the Q parameter of 10, leading to a damping ratio η equal to 0,05. The severity spectral curve, considered individually is not giving any consistent information about the maximal acceleration of the real payload but it needs to be compared to the one relative to the qualification APSD. If it is completely covered by the latter we can be sure that during the tests and the flight the spacecraft will not be affected by damage by any kind of load whose severity is not greater than the one to which the payload was qualified. Otherwise, if some criticality is found during the severity comparison, it will have to be reported in order to remedy the problem during the next design phase.

The severity comparison will be done for the sine, random and shock testing. The methodology to retrieve the severity for each one of the modes is different. Since these three analysis usually tend to share some portions of the frequency spectrum we will probably have in these regions the overlapping of two different severity spectrum curves. In order to compute the severity for the three cases the qualification levels of the unit are needed and are shown in Tab. 8.1:

Test	Frequency range	Qualification level
Sine	$5 < f < 21$ $21 < f < 110$	11 mm 20 g
Random	20 $50 < f < 800$ 2000	$0.01 \text{ } g^2/\text{Hz}$ $0.16 \frac{W}{22.7} \text{ } g^2/\text{Hz}$ $0.01 \text{ } g^2/\text{Hz}$
Shock	100 $2000 < f < 10000$	50 g 800 g

Table 8.1: Qualification loads for the unit

The qualification levels stated in Tab. 8.1 are representative of both in plane and out of plane directions for the load. As it is possible to observe the qualification level for the first part of the sine sweep test frequency range is expressed as a length, in *mm*. The reason for this is that in harmonic motion to each frequency value a sinusoidal amplitude is related. Hence, from the expression of the acceleration as function of time:

$$a(t) = A \sin(2\pi ft) \quad (8.1)$$

The displacement function of the shaker can be obtained by integrating twice eq. 8.1.

$$x(t) = -\frac{A}{4\pi^2 f^2} \sin(2\pi ft) \quad (8.2)$$

where the coefficient multiplying the sine operator is the new maximal amplitude of the motion of the shaker for that frequency. Each shaker device has a maximum allowable displacement, called maximal stroke, which in this case is 11 *mm*. Therefore, starting from this value, the acceleration amplitude can be computed in order to find the qualification acceleration severity of the sine sweep test.

$$\text{Amplitude} = 4D_{stroke}\pi^2 f^2 \quad (8.3)$$

$$SEV(f)_{sine} = \text{Amplitude}(f)Q \quad (8.4)$$

Where Q is equal to the conventional value equal to 10. The computation of the severity for the shock testing is also immediate. The severity g-spectrum of a shock profile is self-evident since a shock profile is already obtained as the SRS of a time-history.

$$SEV(f)_{shock} = SRS(f). \quad (8.5)$$

In order to retrieve the severity related to the random test the Extreme Response Spectrum (ERS) is required, which can be computed using the formula 8.6:

$$ERS(f) = \ddot{u}_{RMS} \sqrt{2\ln(fT)} \quad (8.6)$$

Where \ddot{u}_{RMS} is the root mean square of the maximal acceleration of the single DOF system and T is the duration, expressed in seconds, of the random test. The first quantity can be retrieved in eq. 8.7 by using the transmissibility of the single DOF system:

$$sDOFT_r(f) = \frac{1 + 2i\eta(\frac{f}{f_n})}{1 - (\frac{f}{f_n})^2 + 2i\eta(\frac{f}{f_n})} \quad (8.7)$$

$$\ddot{u}_{RMS} = \sqrt{\int_f |sDOFT_r(f)|^2 APSD(f) df} \quad (8.8)$$

Differently from the sine sweep and shock testing, a statistical approach was needed to compute the severity of the random APSD profile, hence, considering a single DOF system with a specific resonant frequency excited by the above random load , the $ERS(f)$ represents the acceleration value which would be exceeded only once by the mass during the considered amount of time, if the system was subjected to the random load. The same process has to be done for both APSD qualification level and the output of the acoustic load prediction analysis.

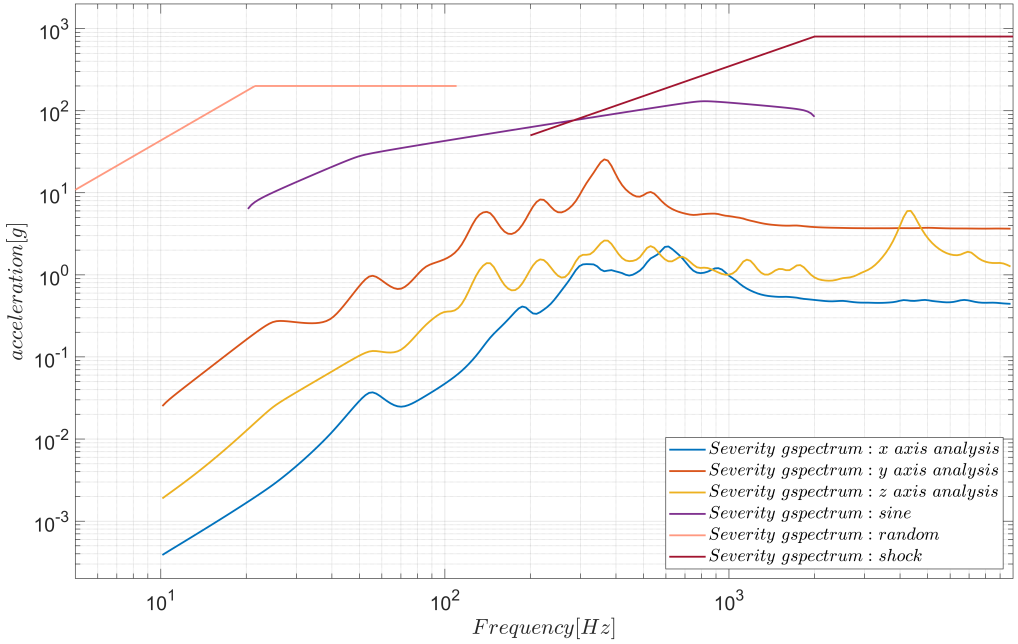


Figure 8.1: Severity comparison

In the chart 8.1 all severity profiles are shown. It is clear that each one of the three simulation outputs are completely covered by all qualification curves, in all the regions including the ones in which two qualification curves are overlapping. If one single curve crossed at least once the qualification level, this would be an indication that in the next design phase a solution to solve this criticality should be found: the unit could be further tested in order to be qualified for higher accelerations, its position could be changed inside the spacecraft or the entire space structure could be modified in order to fulfill the requirement. The results in Fig. 8.1 are quite far from this scenario.

Frequency range	Type of qualification
$5 < f < 20$	sine qualified
$20 < f < 110$	sine and random qualified
$110 < f < 200$	random qualified
$200 < f < 2000$	random and shock qualified
$2000 < f < 10000$	shock qualified

Table 8.2: Severity comparison summary

Chapter 9

Buckling analysis

9.1 Introduction

The structural design is usually based on two criteria:

- **Strength criteria:** ensure that the structure withstand applied loads without failure or deformation beyond acceptable limits;
- **Stiffness criteria:** control deformation and excessive movement by setting limits for deflections, strains and natural frequencies for different loads.

The goal is to strike a balance between strength and stiffness criteria to verify that the structure can safely support loads while maintaining its intended form and function. However, an analysis based only on these two aspects neglects the stability behaviour of the structure and its related phenomena that, if not studied properly, could lead the entire structure to failure.

Buckling is a deformation of a structural member loaded in compression, that occurs when the compressive load in the member reaches a critical value. This behaviour often occurs suddenly, and can produce large displacements. Even though it does not always result in yielding or fracture of the material [6], buckling is still considered to be a failure mode since the buckled structure can no longer support a load in the way it was originally intended to; this is why it shall be assessed carefully in the design phase.

Considering that during its mission the spacecraft undergoes high compressive loads, a buckling analysis of the spacecraft is carried out.

9.2 Buckling model

Firstly, the external loads were taken into account: for this analysis, the QLS from Tab.3.1 were considered. Since this is a buckling analysis, only compressive longitudinal modes were picked, while regarding lateral modes both the directions +X and -X were considered due to the fact that SC is not axial-symmetric. Considering a SF (Safety Factor) of 1.25 [1], the generic load is expressed as:

$$L = QLS \times SF \quad (9.1)$$

The buckling analysis was performed through the MSC Nastran template 105 buckling run code. There are two steps in the procedure sequence:

- **Pre-buckling analysis:** for the pre-buckling problem, the external loads are prescribed and the boundary conditions are set. This is a boundary value problem that, once solved, returns the deformed configuration of the structure and the related internal loads. Regarding the boundary conditions, the SC is constrained through an interface to the LV;
- **Buckling analysis:** the buckling problem is an eigenvalue problem which allows to compute the minimum eigenvalue λ_{min} used to find the buckled configuration. Afterward, it is possible to find the buckling load by multiplying the applied force by λ_{min} . Moreover, once λ_{min} is computed, the MoS (Margin of Safety) is defined:

$$MoS = \lambda_{min} - 1 \quad (9.2)$$

Lastly, it is important to point out that in this case the deformed shape under buckling effect is retrieved through an eigenvalue analysis; in order to obtain the effective deformation, a non-linear analysis is required.

9.3 Results

The minimum eigenvalues λ_{min} for each value of QLS are shown in Tab. 9.1:

QLS_{long} [g]	QLS_{lat} [g]	λ_{min}	MoS
-7.5	0	29.95881	28.95881
-7.5	0.625	28.01055	27.01055
-5	0.625	40.04872	39.04872
-4.375	2.5	28.51616	27.51616
-4.375	-2.5	28.74921	27.74921
-5	-0.625	39.42682	38.42682
-7.5	-0.625	27.55283	26.55283

Table 9.1: QLS and λ_{min} values

All the eigenvalues are positive: this is due to the fact that only compressive loads are included in the analysis. Furthermore, when considering the same value of QLS_{long} , the minimum eigenvalue associated to the load slightly changes depending on the direction of QLS_{lat} : this finds an explanation in the fact that the SC's mass does not follow an axial-symmetric distribution.

Furthermore, it is possible to understand the impact of the compression generated from the bending of the SC on the analysis by looking at the first and second row of Tab. 9.1: for the same longitudinal load, QLS_{lat} is significantly different. However, the value of λ_{min} does not vary sensibly, meaning that the bending of SC has little influence on the compressive load.

Below are reported the deformations of the structure caused by the buckling effect. As reported earlier, they are obtained through an eigenvalue analysis: for this reason, only the node shapes are represented.

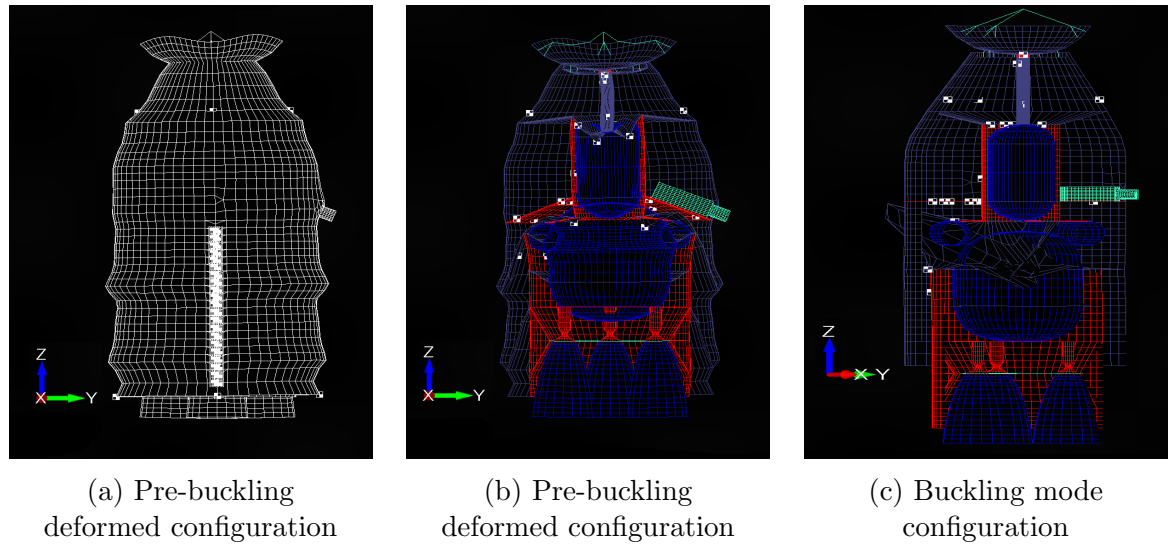


Figure 9.1: Buckling mode: $\lambda_{min} = 29.95881$

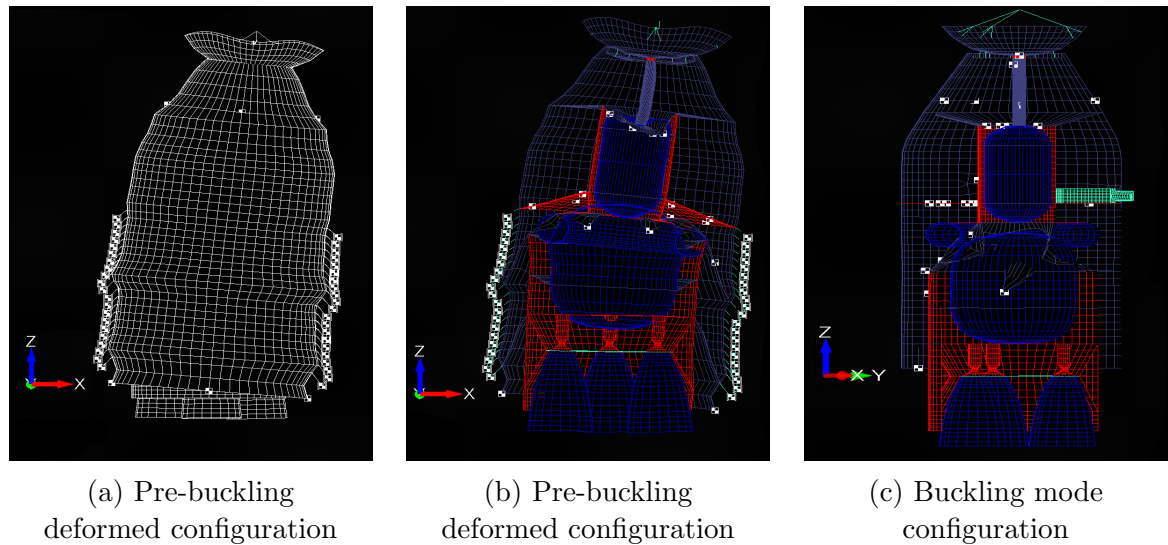


Figure 9.2: Buckling mode: $\lambda_{min} = 28.01055$

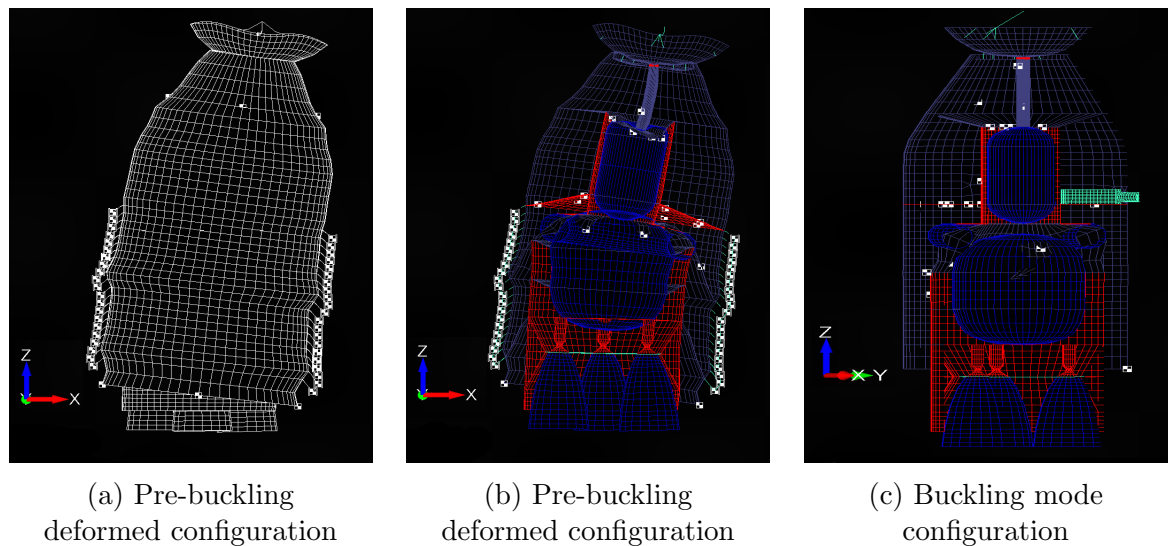


Figure 9.3: Buckling mode: $\lambda_{min} = 40.04872$

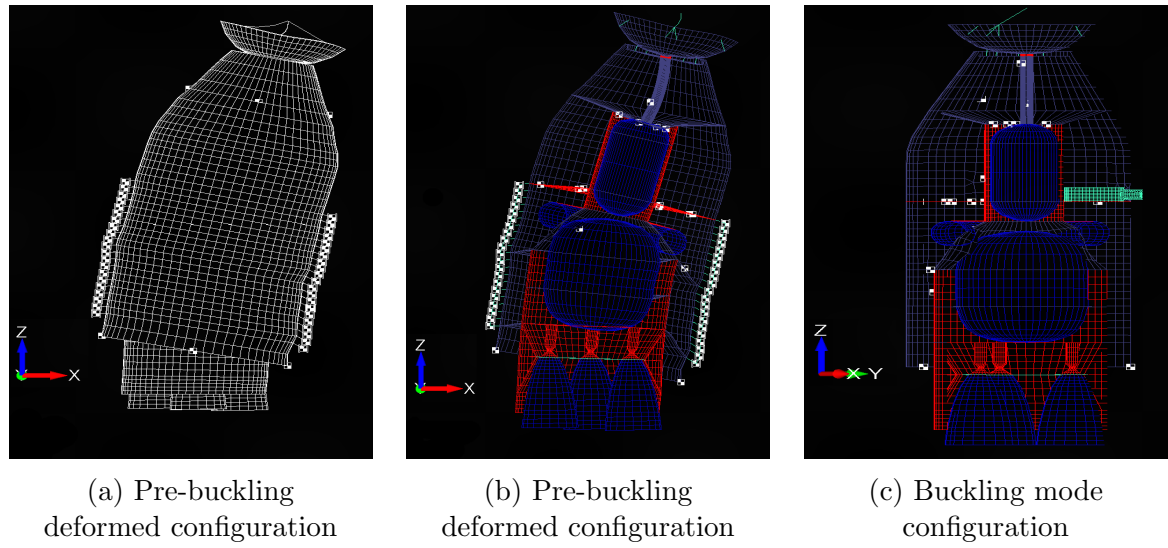


Figure 9.4: Buckling mode: $\lambda_{min} = 28.51616$

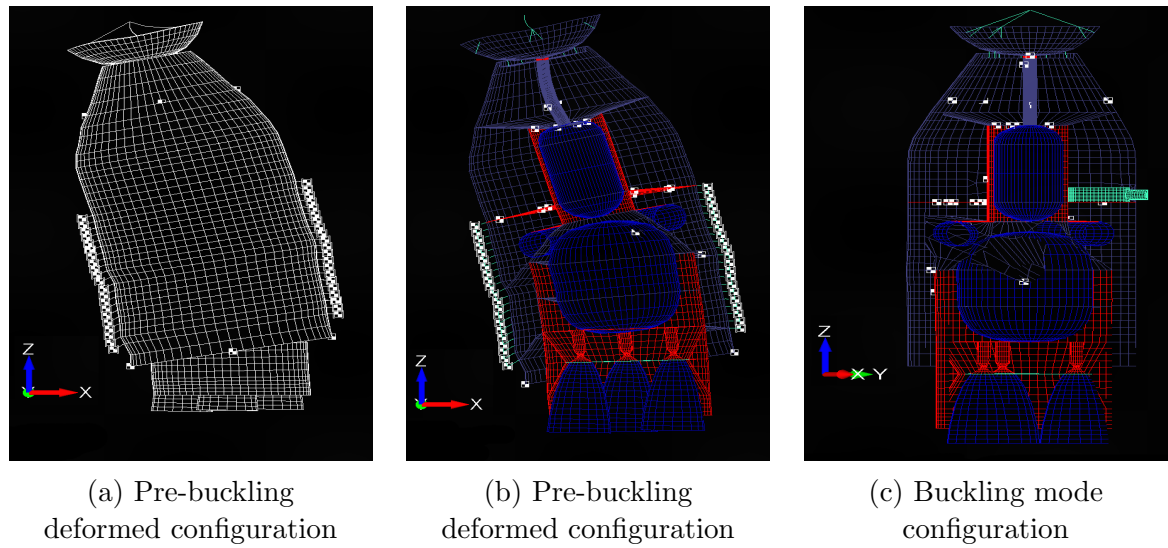


Figure 9.5: Buckling mode: $\lambda_{min} = 28.74921$

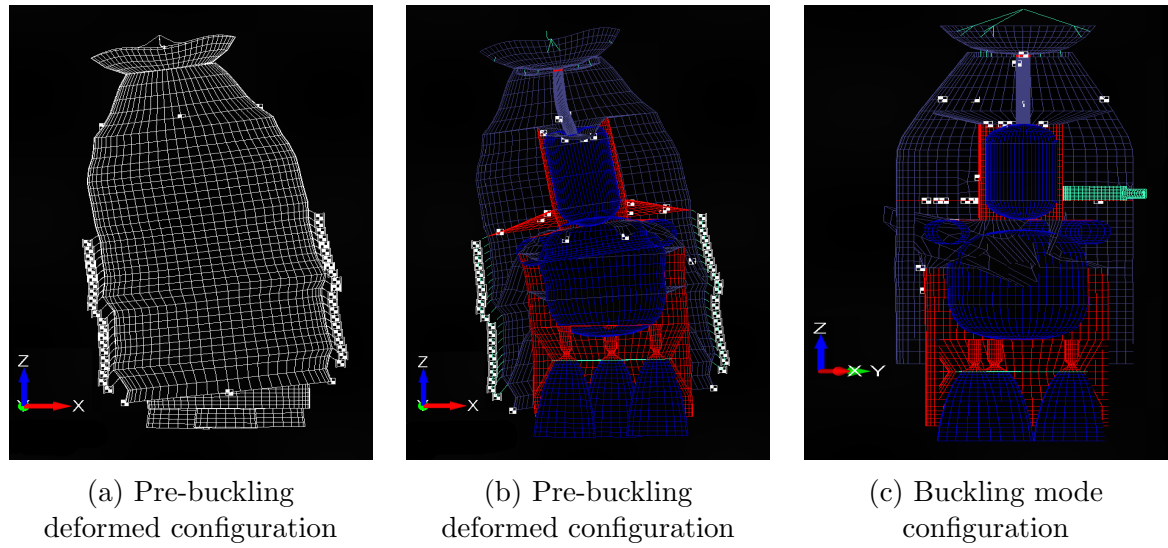
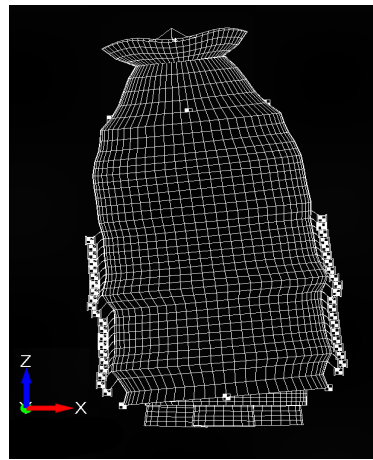
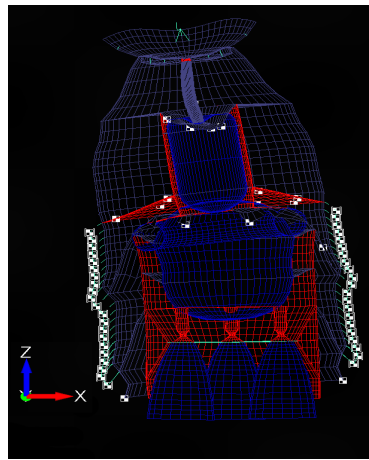


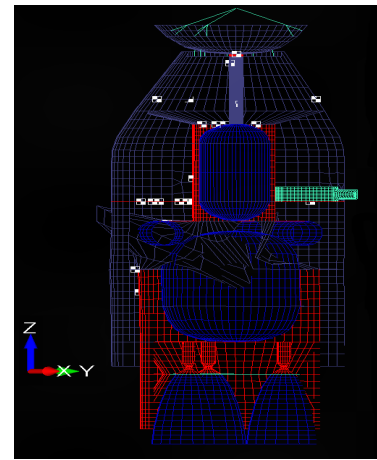
Figure 9.6: Buckling mode: $\lambda_{min} = 39.42682$



(a) Pre-buckling
deformed configuration



(b) Pre-buckling
deformed configuration



(c) Buckling mode
configuration

Figure 9.7: Buckling mode: $\lambda_{min} = 27.55283$

Chapter 10

Summary of requirements

Below, a recapitulation of the fulfillment of the requirements is presented. Eventual criticalities shall be considered during the next design phase.

Requirement	Fulfillment	Additional notes
Fairing volume	Yes	None
Total mass upper and lower limits	Yes	None
Position of COG	Yes	None
Lateral modal frequency	Yes	None
Longitudinal modal frequency	Yes	None
Secondary modal frequency	Yes	None
Overflux limitation below 10 %	Yes	None
Thermoelastic analysis	No	Relative rot. between telescope and sensors are too high
Sine testing	Yes	None
Random testing	Yes	None
Buckling analysis	Yes	None

Table 10.1: Recapitulation of all the analysis

Bibliography

- [1] SpaceX. *Falcon user's guide*. September 2021.
- [2] N. Pietro. *Analysis and testing of space structures lecture notes*. 2023.
- [3] Hexagon. *Msc nastran 2022.3 linear static analysis user's guide*. 2022.
- [4] B. Z. Franco. *Spacecraft attitude dynamics lecture notes*. 2022.
- [5] NASA. *NASA GODDARD SPACE FLIGHT CENTER GENERAL ENVIRONMENTAL VERIFICATION STANDARD (GSFC)*. 2021.
- [6] *Understanding buckling*. URL: <https://efficientengineer.com/buckling/>.